

Structure-Aided Identification and Optimization of Tetrahydro-isoquinolines as Novel PDE4 Inhibitors Leading to Discovery of an Effective Anti-Psoriasis Agent

Xianglei Zhang, Guangyu Dong, Heng Li, Wuyan Chen, Jian Li, Chunlan Feng, Zhanni Gu, Fenghua Zhu, Rui Zhang, Minjun Li, Wei Tang, Hong Liu, and Yechun Xu

J. Med. Chem., **Just Accepted Manuscript** • Publication Date (Web): 17 May 2019

Downloaded from <http://pubs.acs.org> on May 17, 2019

Just Accepted

“Just Accepted” manuscripts have been peer-reviewed and accepted for publication. They are posted online prior to technical editing, formatting for publication and author proofing. The American Chemical Society provides “Just Accepted” as a service to the research community to expedite the dissemination of scientific material as soon as possible after acceptance. “Just Accepted” manuscripts appear in full in PDF format accompanied by an HTML abstract. “Just Accepted” manuscripts have been fully peer reviewed, but should not be considered the official version of record. They are citable by the Digital Object Identifier (DOI®). “Just Accepted” is an optional service offered to authors. Therefore, the “Just Accepted” Web site may not include all articles that will be published in the journal. After a manuscript is technically edited and formatted, it will be removed from the “Just Accepted” Web site and published as an ASAP article. Note that technical editing may introduce minor changes to the manuscript text and/or graphics which could affect content, and all legal disclaimers and ethical guidelines that apply to the journal pertain. ACS cannot be held responsible for errors or consequences arising from the use of information contained in these “Just Accepted” manuscripts.

1
2
3
4 **Structure-Aided Identification and Optimization of Tetrahydro-**
5
6
7 **isoquinolines as Novel PDE4 Inhibitors Leading to Discovery of an**
8
9 **Effective Anti-Psoriasis Agent**
10

11
12
13
14 Xianglei Zhang,^{Δ,§,†} Guangyu Dong,^{§,‡,†} Heng Li,^{Δ,§,†} Wuyan Chen,^Δ Jian Li,^Δ Chunlan
15
16
17 Feng,^Δ Zhanni Gu,^Δ Fenghua Zhu,^Δ Rui Zhang,^{Δ,§} Minjun Li,[‡] Wei Tang,^{Δ,§,*} Hong
18
19
20 Liu,^{Δ,§,*} and Yechun Xu^{Δ,§,*}
21

22 ^ΔCAS Key Laboratory of Receptor Research, State Key Laboratory of Drug
23
24 Research, Drug Discovery and Design Center, Laboratory of
25
26
27 Immunopharmacology, Shanghai Institute of Materia Medica, Chinese Academy of
28
29
30 Sciences, Shanghai 201203, China
31

32
33 [§]University of Chinese Academy of Sciences, Beijing 100049
34

35
36 [‡]School of Life Science and Technology, ShanghaiTech University, Shanghai
37
38
39 201210, China
40

41
42 [†]Shanghai Synchrotron Radiation Facility, Shanghai Advanced Research Institute,
43
44
45 Chinese Academy of Sciences, Shanghai 201210, China
46
47

48 **ABSTRACT**
49

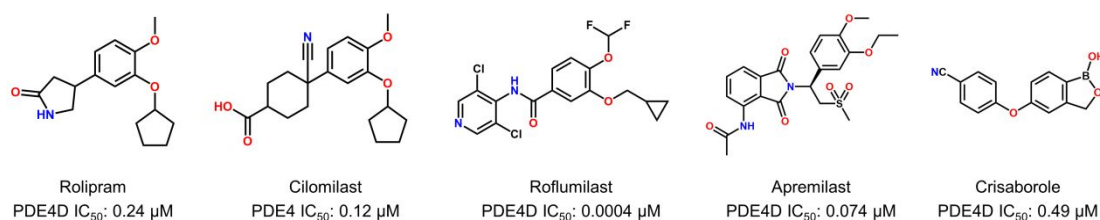
50
51
52 Psoriasis is a common, chronic inflammatory disease characterized by abnormal skin
53
54
55 plaques, and the effectiveness of PDE4 inhibitor to lessen the symptoms of psoriasis
56
57
58 has been proved. Aiming to find a novel PDE4 inhibitor acting as an effective, safe and
59
60

1
2
3
4 convenient therapeutic agent, we constructed a library consisting of berberine analogs
5
6
7 and compound **2** with a tetrahydro-isoquinoline scaffold was identified as a novel and
8
9
10 potent hit. The structure-aided and cell-based SAR studies on a series of tetrahydro-
11
12 isoquinolines lead to efficient discovery of a qualified lead compound (**16**) with the
13
14 high potency and selectivity, well-characterized binding mechanism, high cell-
15
16 permeability, good safety and pharmacokinetic profile, and impressive in vivo efficacy
17
18 on anti-psoriasis in particular with a topical application. Thus, our study presents a
19
20 prime example for efficient discovery of novel, potent lead compounds derived from
21
22 natural products using a combination of medicinal chemistry, biochemical, biophysical,
23
24 and pharmacological approaches.
25
26
27
28
29
30

31 32 INTRODUCTION

33
34
35
36 Cyclic nucleotide phosphodiesterases (PDEs) catalyse the hydrolysis of cAMP and
37
38 cGMP, regulating the cAMP- and cGMP-associated signalling pathways as well as the
39
40 resulting physiological and pathophysiological responses, and they are proving to be
41
42 fruitful targets for drug discovery.¹⁻³ PDE4, one of the 11 known human PDEs,
43
44 specifically catalyzes the hydrolysis of cAMP which in turn interferes with the function
45
46 of transcription factors like CREB and NF- κ B, altering the expression of inflammatory
47
48 mediators such as TNF- α , IFN- γ , IL-12, and IL-10.^{4,5} Moreover, PDE4 isoforms
49
50 (PDE4A/4B/4C/4D) have a relatively high level of expression in cells that regulate
51
52 inflammatory responses.⁶ Accordingly, therapeutic benefits of PDE4 inhibitors have
53
54
55
56
57
58
59
60

1
2
3
4 been used in the treatment of inflammatory diseases including chronic obstructive
5
6 pulmonary disease (roflumilast), psoriasis (apremilast) and atopic dermatitis
7
8 (crisaborole) (Figure 1).⁷⁻¹⁰ Given the effectiveness of the target for antiinflammation,
9
10 there is considerable interest in the discovery of novel PDE4 inhibitors.
11
12
13



23 **Figure 1.** Structures and inhibitory activities of berberine and representative PDE4
24 inhibitors including three approved drugs (roflumilast, apremilast and crisaborole).
25
26
27
28
29

30 Psoriasis is a common, chronic skin disease with a prevalence of ~2% worldwide.¹¹
31
32 It has been recognized as an immune-mediated genetic disease or a systemic
33 inflammatory disease manifested as raised, well-demarcated, erythematous oval
34 plaques with adherent silvery scales.¹² Conventional therapies include topical therapies
35 and biologics. Glucocorticosteroids are common topical agents for psoriasis treatment,
36 however, the side effect of skin atrophy hinders its long-term use. Although several
37 biologics including etanercept, adalimumab and infliximab have been approved for the
38 treatment of psoriasis and psoriatic arthritis, they are expensive and require either
39 subcutaneous or intravenous administration.¹³ There is a substantial unmet need for the
40 treatment of psoriasis with cheaper oral drugs or safer topical agents. Apremilast, an
41 oral small-molecule PDE4 inhibitor, was approved by the FDA in 2014 for the
42 treatment of moderate-to-severe plaque psoriasis.¹⁴ Crisaborole, another PDE4
43
44
45
46
47
48
49
50
51
52
53
54
55
56
57
58
59
60

1
2
3
4 inhibitor, used as a topical medication for the treatment of mild-to-moderate atopic
5
6 dermatitis was also approved by the FDA in 2016.^{10,15} It prompts us to seek a new
7
8
9 therapeutic agent for psoriasis targeting PDE4.
10

11
12 Traditional Chinese medicine (TCM) has evolved over thousands of years and is
13
14 an invaluable source of inspiration for drug discovery. The therapeutic benefits of TCM
15
16 led us to extract its active components, the vast majority of which are natural products,
17
18 as lead compounds for drug development.¹⁶ Berberine (BBR), the major active
19
20 ingredient of *Coptis chinensis*, is a small-molecule alkaloid and is broadly used as an
21
22 antimicrobial drug.^{17,18} Mounting evidence also suggests that BBR has a promising
23
24 pharmacological efficacy on inflammation.¹⁹⁻²¹ It has been reported that BBR processes
25
26 anti-inflammatory activities and suppresses pro-inflammatory responses by inhibition
27
28 of mitogen-activated protein kinase (MAPK) signalling and cellular reactive oxygen
29
30 species (ROS) production, although the full range of biological target(s) of BBR
31
32 remains unclear.²² In addition, BBR possesses a typical catechol group, which is a
33
34 common pharmacophore in known PDE4 inhibitors (Figure 1). Therefore, we built a
35
36 chemical library consisting of precursors, intermediates and various derivatives of
37
38 berberine in order to discover a new scaffold PDE4 inhibitor for the treatment of
39
40 psoriasis (Figure 2).
41
42
43
44
45
46
47
48
49
50
51

52 53 54 **RESULTS AND DISCUSSION** 55 56 57 58 59 60

1
2
3
4 **Hit Discovery and Chirality Identification.** At the outset of our project, we used
5
6
7 virtual screening to efficiently dig out hit compounds from our in-house BBR analogues
8
9
10 library. The top 30 compounds ranked by scoring values were subsequently evaluated
11
12 for inhibitory activity on PDE4D by a scintillation proximity assay (SPA).²³ Among
13
14 these compounds, we found a tetrahydro-isoquinoline-based compound (compound **1**)
15
16 as a novel scaffold inhibitor of PDE4. It turned out to be a racemic compound with an
17
18 IC₅₀ of 0.51 μM. We synthesized and soaked the racemic entity with apo crystals of the
19
20 catalytic domain of PDE4D, determining the complex structure of PDE4D-**1** (Scheme
21
22
23 1 and Table S1, PDB code: 6INM). It revealed that the (*S*)-enantiomer occupied the
24
25 active site of PDE4D (Figure S1). A further separation and purification of two
26
27 enantiomers followed by the SPA-based activity assessment indicated that (*S*)-
28
29 enantiomer (compound **2**) is more potent than (*R*)-enantiomer (compound **3**), with an
30
31 IC₅₀ of 0.27 μM and 3.71 μM, respectively (Scheme 1). We further solved the crystal
32
33 structure of PDE4D soaked with the (*S*)-enantiomer which results in a binding
34
35 conformation of the compound nearly identical to that in the PDE4D-**1** complex, but
36
37 we were unable to obtain the crystals of PDE4D bound with the (*R*)-enantiomer (Figure
38
39 S1 and Table S1, PDB code: 6INK). As confirmed by the SPA assay together with the
40
41 proof for the binding conformation of the ligand in the crystal structures, compound **2**
42
43
44 was identified as a good hit for further optimization.
45
46
47
48
49
50
51
52
53
54
55
56
57
58
59
60

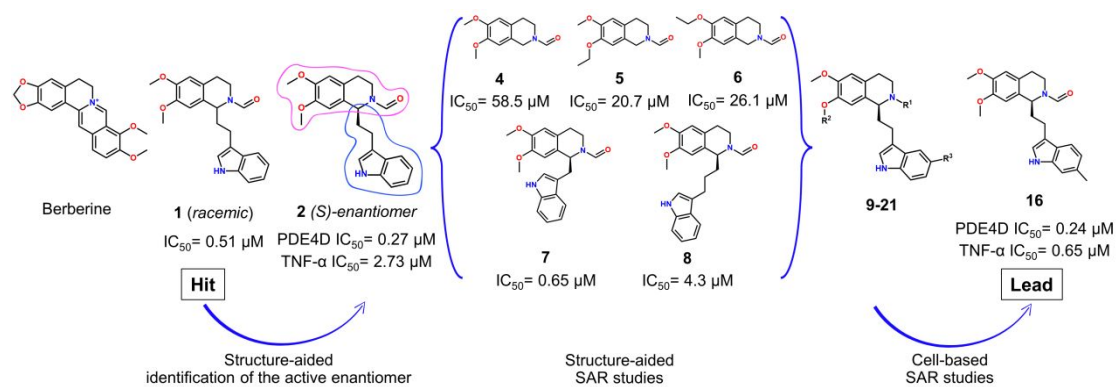
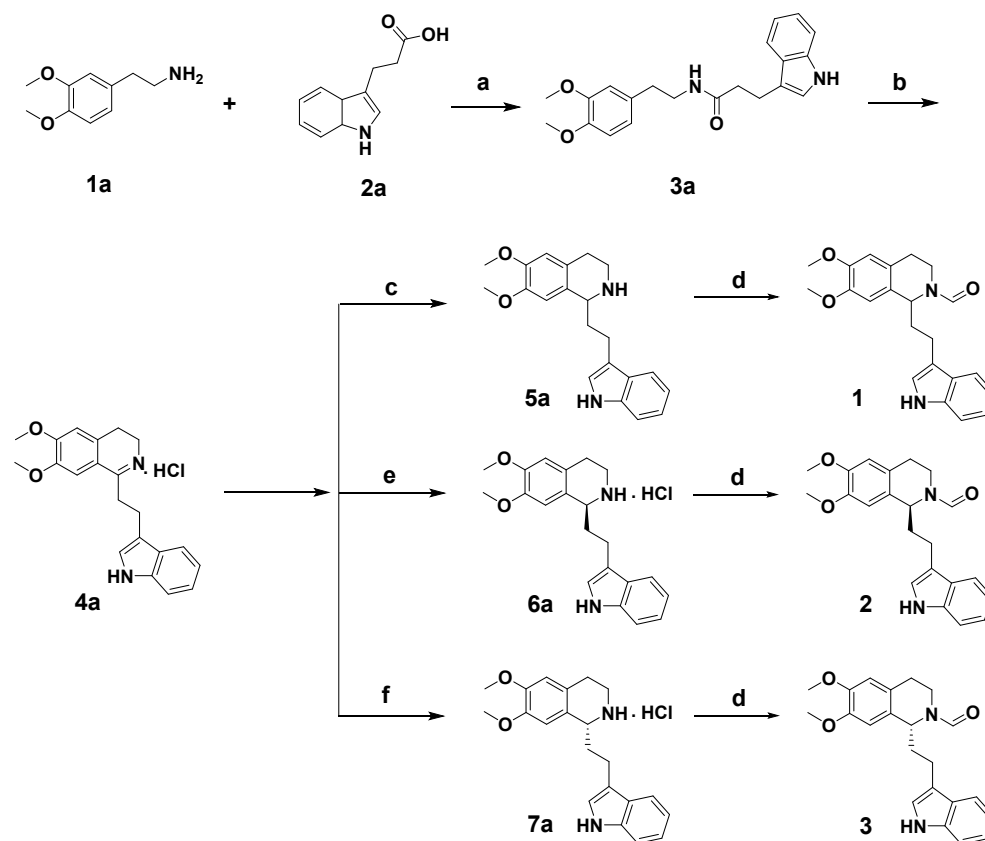


Figure 2. Structure-aided and cell-based discovery and design of the lead compound (16) based on an in-house BBR analogues library.

Scheme 1. Synthesis Route of Compounds 1-3.



Reagents and conditions: (a) EDCI, HOBT, TEA, rt, DCM, 80-90%; (b) POCl₃, CH₃CN reflux, 90-95%; (c) NaBH₄, MeOH, 82%; (d) HCOOEt, TEA reflux, 72-85%; (e) RuCl[(*R,R*)-Tsdpen](*p*-cymene), AgSbF₆, La(OTf)₃, HCOONa, H₂O/MeOH= 2:1, Ar,

1
2
3
4 40°C, 65-73%; (f) RuCl[(*S,S*)-Tsdpen](*p*-cymene), AgSbF₆, La(OTf)₃, HCOONa,
5
6 H₂O/MeOH = 2:1, Ar, 40°C, 65-73%.
7
8
9

10 **Structure-Aided SAR Studies on Substituents of the Tetrahydro-isoquinoline**

11 **Ring.** In order to efficiently carry out the hit-to-lead optimization, it is of utmost
12 importance to understand the underlying structure-activity relationship (SAR) of
13 tetrahydro-isoquinolines binding with PDE4D. In addition, compound **2** possesses an
14 excellent potency with a submicromolar IC₅₀. It is thus interesting to evaluate
15 contribution of each functional group of the scaffold to binding and inhibition of
16 PDE4D. To this end, the flexible “tail” (the indole ring attached with the ethylidene)
17 was removed from **2** to yield a fragment only containing the tetrahydro-isoquinoline
18 core (compound **4**) (Figure 2). The crystal structure determination revealed that
19 compound **4** could bind into the pocket of PDE4D with two orientations associated with
20 hydrogen bond (H-bond) formation or not between the carbonyl group and H160
21 (Figure 3A and Table S1, PDB codes: 6IMB and 6IMD). This is consistent with the
22 thermodynamic profile of **4** determined by isothermal titration calorimetry (ITC) that it
23 has a relatively weak binding enthalpy while its entropic contribution is favourable
24 (Table S2). It is not difficult to understand that the lack of the “tail” and the existence
25 of two identical methoxyl groups allow the tetrahydro-isoquinoline ring to adopt two
26 different bound conformations in the enzyme. However, the complex structures
27 together with the thermodynamic data suggest that interaction of the carbonyl group
28 with H160 is not sufficient to fix the binding conformation of **4**. To further validate and
29
30
31
32
33
34
35
36
37
38
39
40
41
42
43
44
45
46
47
48
49
50
51
52
53
54
55
56
57
58
59
60

1
2
3
4 understand it, we designed and synthesized compounds **5** and **6** by replacement of each
5
6 methoxyl group of **4** with an ethoxyl one (Figure 2 and Scheme 2). The solved crystal
7
8 structures show that the ethoxyl group of **5** or **6** always inserts into a hydrophobic sub-
9
10 pocket, named the Q-pocket, formed by the sidechains of N321, Y329, T333, and I336,
11
12 playing a key role in determination of the binding conformation of the compounds
13
14 (Figure 3B,C and Table S1, PDB codes: 6IM6 and 6IMI). Similar to what was found
15
16 with two bound conformations of **4**, the carbonyl group of **5** makes the H-bond to H160
17
18 with a distance of 2.7 Å while such a H-bond is not established in the case of **6** (Figure
19
20 S2). In addition, superimposition of the structures of **4**, **5** and **6** suggests that a small
21
22 shift of the tetrahydro-isoquinoline ring of **5** towards the solvent region results in
23
24 stronger π - π stacking interactions with F372 (Figure S2). These underlying interactions
25
26 lay a solid foundation for the fact that inhibition of **5** and **6** to PDE4D is much improved
27
28 compared to **4** and the activity of **5** is higher than that of **6** (Figure 2). Moreover, the
29
30 hydrophobic interactions of the methoxyl or ethoxyl group with the Q-pocket and the
31
32 H-bond of the carbonyl group to H160 both contribute to binding of the tetrahydro-
33
34 isoquinoline core to PDE4D, although the former is more significant than the latter. As
35
36 a result, compound **5** with a best inhibitory activity among three fragments and a similar
37
38 binding conformation to the tetrahydro-isoquinoline of compound **2** provides a good
39
40 candidate for further optimization.
41
42
43
44
45
46
47
48
49
50
51
52
53
54
55

56 **Scheme 2. Synthesis Route of Compounds 4-6.**

57
58
59
60

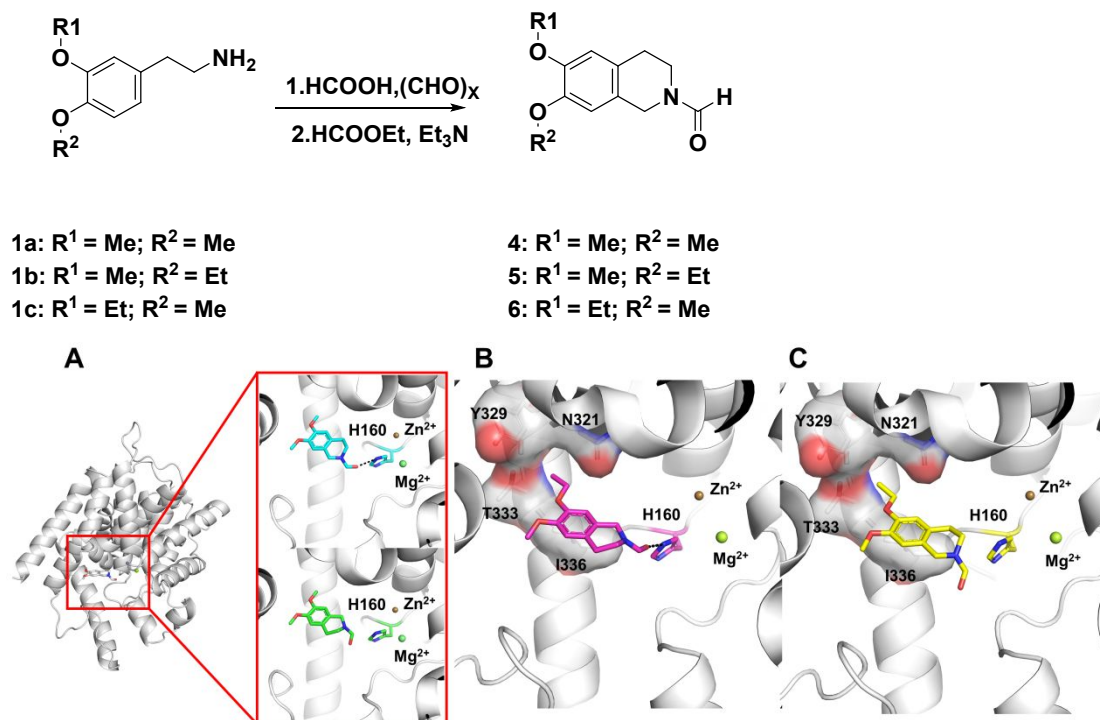


Figure 3. Crystal structures of the catalytic domain of PDE4D in complex with compounds **4** (cyan and green, PDB codes: 6IMB and 6IMD), **5** (magenta, PDB code: 6IM6) and **6** (yellow, PDB code: 6IMI). (A) Two opposite orientations of **4** were found in the binding pocket of PDE4D. (B,C) The ethoxyl groups of **5** and **6** both insert into a hydrophobic sub-pocket (the Q-pocket) formed by the sidechains of N321, Y329, T333, and I336 (grey surface). Dash lines indicate H-bonds between compounds and residues.

Structure-Aided SAR Studies on the “Tail”. The IC₅₀ of **4** is 58.5 μM, which is >200-fold drop in activity relative to compound **2**, suggesting that the “tail” which includes the indole ring and the ethylidene group exerts a significant influence on inhibition of **2** to PDE4D (Figure 2). Analysis of the crystal structure of PDE4D-**2** shows the terminal indole ring is not well fixed and it forms few hydrophobic interactions with residues

1
2
3
4 M273 and M357 (Figures 4A and S1). Moreover, occupation of the solvent accessible
5
6 region by the “tail” leads to the release of water molecules from the binding pocket
7
8 (Figure S3). These binding features result a dramatic entropic contribution to the
9
10 binding affinity of **2** to PDE4D (Table S2). These data make us to speculate that the
11
12 length of the linker between two rings may affect flexibility of the compound and the
13
14 binding of the indole ring with surrounding residues. In view of this, we changed the
15
16 linker between the indole ring and the tetrahydro-isoquinoline ring, i.e. the ethylidene
17
18 in **2** replaced by a methylene and propylidene in compounds **7** and **8**, respectively. The
19
20 IC₅₀ values of **7** and **8** are 0.65 μM and 4.3 μM, respectively, demonstrating that
21
22 shortening or lengthening of the linker does not improve the inhibitory activity.
23
24 Analysis of crystal structures of PDE4D in complex with **2**, **7** and **8** shows the indole
25
26 ring of **7** adopts a similar orientation to that of **2** but in the case of **8** it shifts into a well-
27
28 defined hydrophobic sub-pocket formed by M273, H276, H315, and I376 (Figures 4
29
30 and S4, and Table S1; PDB codes: 6IMO and 6IMR). A short linker in **7** or the
31
32 additional hydrophobic interactions to **8** both reduces the mobility of the indole ring,
33
34 which is in line with the reduced entropic contribution to the binding affinities of **7** and
35
36 **8** to PDE4D (Table S2). Additionally, the carbonyl group of the tetrahydro-isoquinoline
37
38 ring of **7** and **8** forms either no, or a weak H-bond to H160, respectively (Figures 4B,C
39
40 and S4). Taken together, these results suggest that the “tail” group has a profound
41
42 influence on the binding affinity of **2** and an optimal linker between two rings is the
43
44 ethylidene for keeping potency of the compound.
45
46
47
48
49
50
51
52
53
54
55
56
57
58
59
60

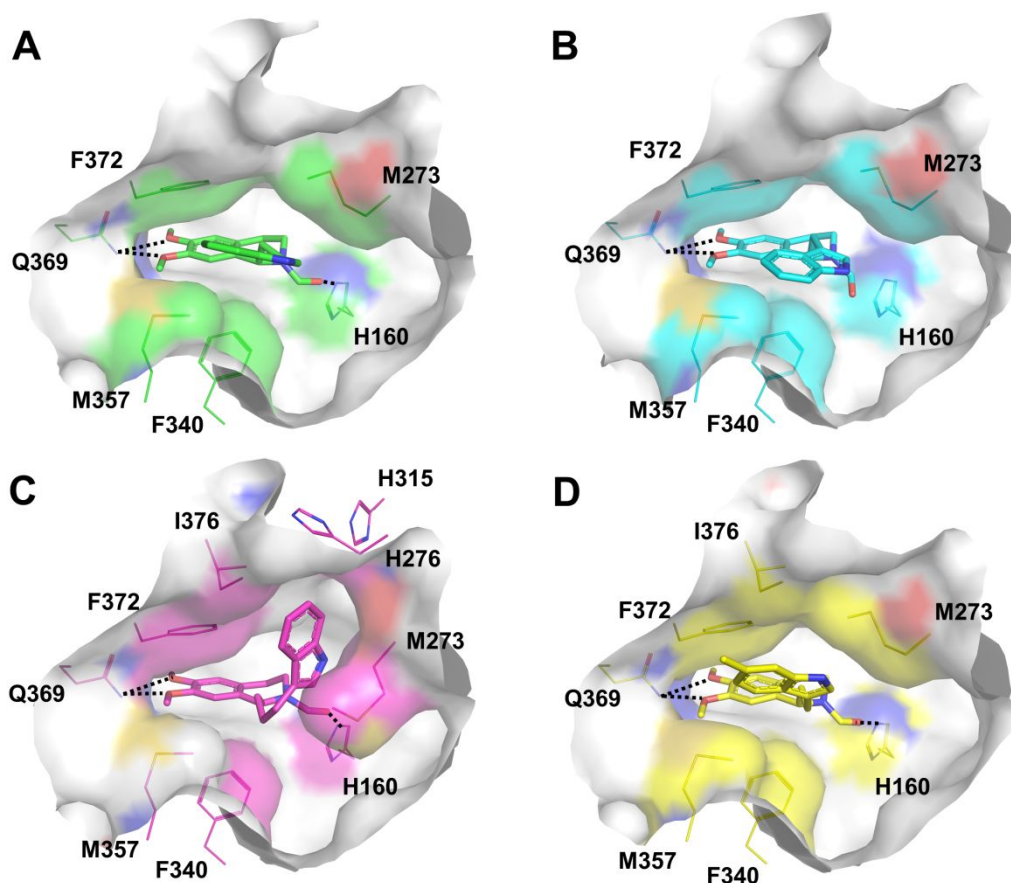


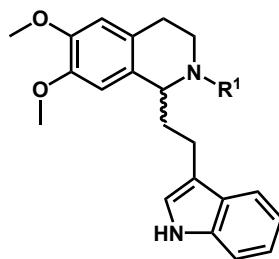
Figure 4. The effect of different linkers on orientations of the indole ring. Surface representation of the PDE4-2 (cyan, A, PDB code: 6INK), PDE4-7 (magenta, B, PDB code: 6IMO), PDE4-8 (green, C, PDB code: 6IMR), and PDE4-16 (yellow, D, PDB code: 6IND) complexes. Dash lines indicate H-bonds between compounds and residues.

Hit-to-Lead Optimization. After fully understanding the binding signature of each part of compound **2**, we decided to keep the ethylidene linker between the tetrahydroisoquinoline ring and the indole ring, and only carry out minor modifications on two rings to improve the enzymatic as well as the cell-based activities (Tables 1 and 2). It has been well demonstrated that elevated levels of cAMP by inhibition of PDE4 would reduce the release of TNF- α , a key cytokine in the inflammatory cascade, from activated

1
2
3
4 monocytes and human peripheral blood mononuclear cells (hPBMC).²⁴ The TNF- α
5
6
7 production in lipopolysaccharide (LPS) stimulated hPBMC was thereby measured
8
9
10 using an enzyme linked immunosorbent assay to evaluate inhibition of compounds to
11
12 PDE4 in cells.

13
14
15 The multiple crystal structures described above show that the carbonyl group of
16
17
18 our compounds has two orientations with or without the H-bond to H160 and it seems
19
20
21 that the contribution of this group to the binding of compounds to PDE4D is not
22
23
24 efficient. Given that this group faces to and is close to two metal ions in the binding
25
26
27 pocket, it is possible to introduce a larger group to form interactions with the metal ions,
28
29
30 like the binding of roflumilast to PDE4D (Figures 1 and S5). We thereby synthesized
31
32
33 compounds **9-14** by introducing the isonicotinoyl (**9**), tetrahydro-2H-pyran-4-carbonyl
34
35
36 (**10**), (tetrahydro-2H-pyran-4-yl)methyl (**11**), 2,2,2-trifluoroethyl (**12**), 2-methoxy-2-
37
38
39 oxoethyl (**13**), or 2-methoxyethyl (**14**) to replace the carbonyl group of compound **1**
40
41
42 (Table 1). Unexpectedly, all compounds showed a significant decreased potency to
43
44
45 PDE4D compared to **1**. Accordingly, the substitution at R¹ position was not favourable
46
47
48 for potency improvement and we keep the carbonyl group in the next optimization steps.

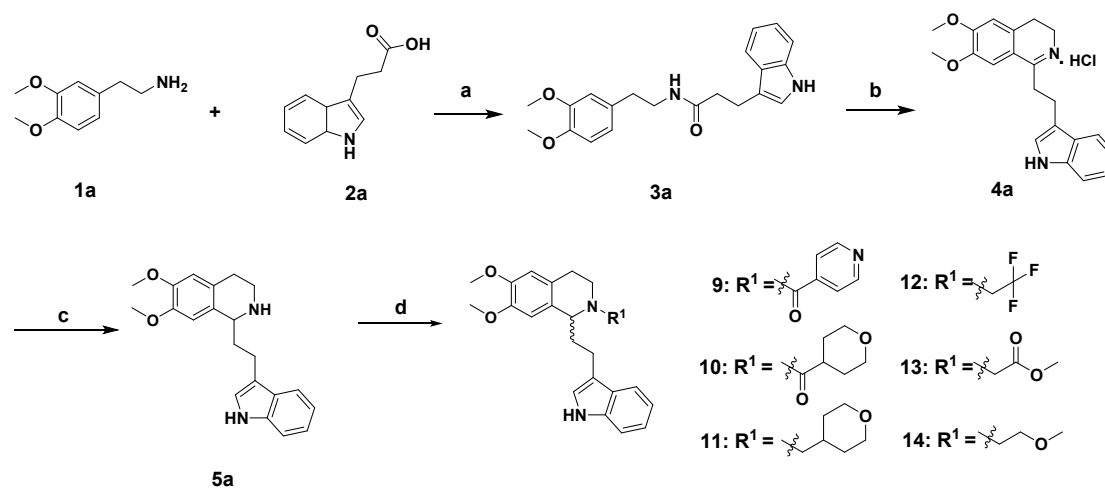
49 **Table 1. Chemical Structures of Compounds 9-14 and Their Inhibitory Activities**
50
51 **against PDE4D and TNF- α Release from hPBMC Stimulated with LPS.**
52
53
54
55
56
57
58
59
60



Comps	R ¹	PDE4D inhibition (1 μM)	TNF-α inhibition (1 μM)
9		30.7%	39.8%
10		16.4%	33.3%
11		34.6% @ 10 μM	36.7% @ 10 μM
12		19.5%	N/A ^a
13		39.1%	21.7%
14		19.2%	25.7% @ 10 μM

^aNot available.

Scheme 3. Synthesis Route of Compounds 9-14.



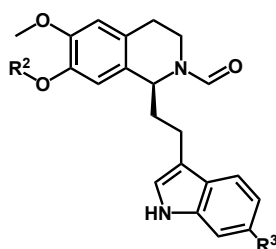
1
2
3
4 Reagents and conditions: (a) EDCI, HOBt, TEA, rt, DCM, 80-90%; (b) POCl₃, CH₃CN
5
6
7 reflux, 90-95%; (c) NaBH₄, MeOH, 82%; (d) (e) R'X /R'OTf, KI, K₂CO₃, CH₃CN,
8
9
10 reflux or R''COX, TEA, DCM or R''COOH, EDCI, DMAP, DCM.
11
12

13
14 As mentioned above, the indole ring of compound **2** oriented towards a
15
16 hydrophobic region but had few interactions with surrounding residues (Figures 4A, S1
17
18 and S6). To increase hydrophobic interactions of the indole ring with residues, we
19
20 added a fluorine (**15**) or a methyl group (**16**) to the indole ring first (Scheme 4).
21
22 Determination of complex structures of **15** and **16** with PDE4D shows that the indole
23
24 rings of two compounds formed more hydrophobic interactions with residues compared
25
26 to **2** (Figure S6, PDB codes: 6IMT and 6IND), which is in line with a higher enthalpic
27
28 contribution of **16** over **2** to the binding affinity of the compound with the enzyme
29
30 (Table S2). The enzymatic IC₅₀ of **15** and **16** is 0.25 and 0.24 μM, respectively, which
31
32 is slightly better than that of **2** (0.27 μM). Surprisingly, compound **16** has a significant
33
34 inhibition on the TNF-α release in hPBMC, yielding an IC₅₀ of 0.65 μM. It is more
35
36 potent than **2** or **15** (Table 2). Given that PDE4 is an intracellular target, the enzymatic
37
38 and cell-based activities of **2**, **15** and **16** indicate that the intrinsic physicochemical
39
40 property of compound **16** may enable it to be more permeable, which is further
41
42 validated by a cell permeability experiment. The data in Table 3 show that both
43
44 compound **16** and apremilast possess a perfect cell-penetrating ability.
45
46
47
48
49
50
51
52
53
54
55
56
57
58
59
60

1
2
3
4 Encouraged by the good potency of **16** in cells, we carried out further modification
5
6 on this compound. The aforementioned structure-aided SAR studies on substituents of
7
8 the tetrahydro-isoquinoline ring have suggested that the ethyl group at R² position is
9
10 better than the methyl one to fit into the Q-pocket and thus improves the inhibitory
11
12 activity of compound **5** as compared to **4**. In addition, in the representative PDE4
13
14 inhibitors shown in Figure 1 imply that a group larger than the ethyl group, such as a
15
16 cyclopropylmethyl or a cyclopentyl, is also possible to be used as substituents of R².
17
18 Therefore, an ethyl group, a cyclopropylmethyl, and a cyclopentyl were introduced at
19
20 the R² position of compounds **17**, **18** and **19**, respectively. As anticipated, the use of
21
22 the ethyl group increased the inhibitory activity of **17** on PDE4D at the enzymatic level.
23
24 Its IC₅₀ is 0.098 μM which is about 3-fold potent of **16**. The cyclopropylmethyl in **18**
25
26 and the cyclopentyl group in **19**, in particular the latter, seem too large for the Q-pocket
27
28 as their enzymatic activities reduced one by one in comparison with **17** or **16**. One
29
30 possibility is that these large hydrophobic groups may compete with the phenyl ring of
31
32 the indole for the same space, and one group pushes the other out of alignment and so
33
34 binding is lost. Unfortunately, the potency of three compounds in hPBMC is all worse
35
36 than compound **16**. Furthermore, we designed and synthesized compounds **20** and **21**
37
38 in which an ethyl group and a cyclopropylmethyl were installed at R², respectively, and
39
40 a hydrogen was used at R³. The enzymatic IC₅₀ of **20** is better than **16** but is worse than
41
42 **17** and meanwhile **21** shows a decreased potency to PDE4D compared to **18**, which are
43
44 consistent with the above SAR studies. However, the potency of **20** and **21** on the TNF-
45
46
47
48
49
50
51
52
53
54
55
56
57
58
59
60

α release in hPBMC is also worse than **16**, demonstrating again the importance of the methyl group at the indole ring for **16** to maintain its potency in cells. Eventually, compound **16** was selected for further evaluation of selectivity, pharmacokinetics and in vivo efficacy.

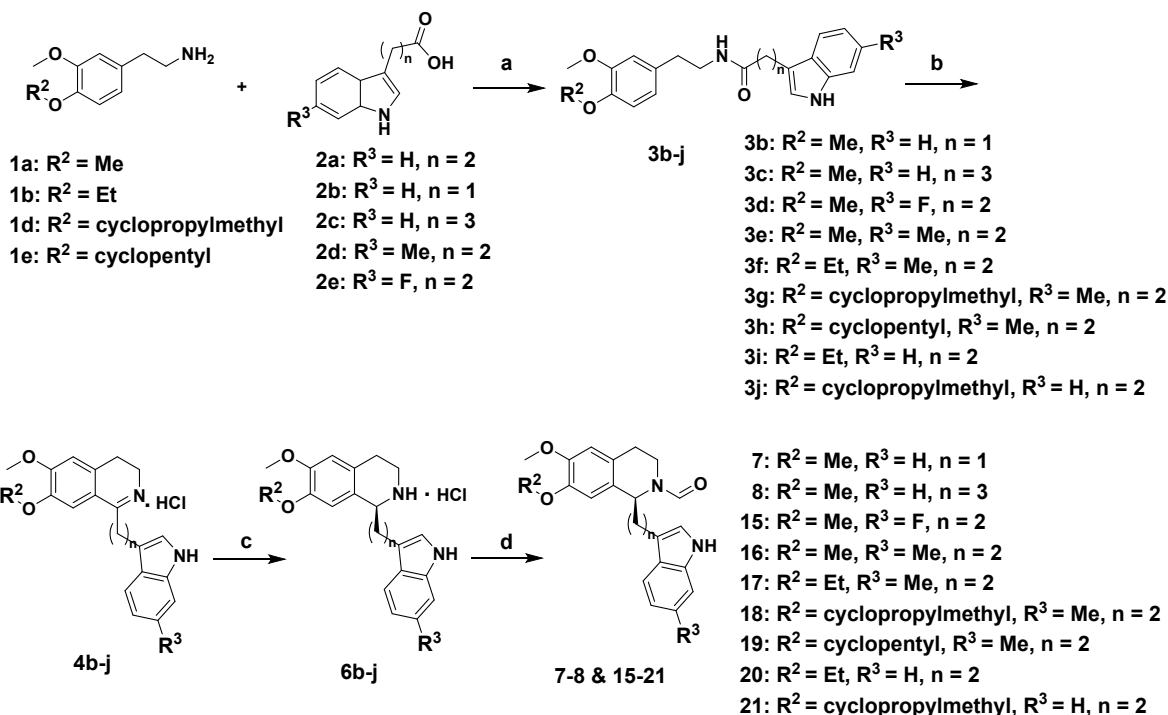
Table 2. Impact of R²- and R³-Substituents on Enzymatic (PDE4D) Activity and Inhibition of TNF- α Release from hPBMC Stimulated with LPS.



Compds	R ²	R ³	PDE4D IC ₅₀ (μM)	TNF- α IC ₅₀ (μM)
apremilast	-	-	0.074 ^a	0.11 ^a
crisaborole	-	-	0.49 ^b	0.54 ^b
2	Me	H	0.27 ± 0.01	2.73 ± 0.17
15	Me	F	0.25 ± 0.003	5.83 ± 1.72
16	Me	Me	0.24 ± 0.02	0.65 ± 0.12
17	Et	Me	0.098 ± 0.004	36.5% @ 1 μM
18		Me	0.70 ± 0.01	2.16 ± 0.04
19		Me	24% @ 1 μM	12.1% @ 1 μM
20	Et	H	0.13 ± 0.01	2.71 ± 0.70
21		H	0.82 ± 0.17	2.58 ± 0.72

^{a,b}The inhibitory activity data of apremilast and crisaborole are cited from references.^{14,25}

Scheme 4. Synthesis Route of Compounds 7-8 and 15-21.



Reagents and conditions: (a) EDCI, HOBT, TEA, rt, DCM, 80-90%; (b) POCl₃, CH₃CN reflux, 90-95%; (c) RuCl[(*R,R*)-Tsdpen](*p*-cymene), AgSbF₆, La(OTf)₃, HCOONa, H₂O/MeOH= 2:1, Ar, 40 °C, 65-73%, (d) HCOOEt, TEA reflux, 72-85%.

Table 3. Cell Permeability Results of Compound 16 and Apremilast.

Compds	Flow Direction	Mean Recovery (%)	Mean P _{app} ^a (10 ⁻⁶ cm/s)	Mean F _{abs} ^b (%)	Efflux Ratio ^c	Permeability class ^d
apremilast	apical to basal	96.68 ± 4.81	14.93 ± 1.27	100	1.9	high
apremilast	basal to apical	92.12 ± 2.78	29.02 ± 1.33			
16	apical to basal	92.27 ± 2.51	18.43 ± 0.70	100	1.1	high
16	basal to apical	96.84 ± 0.27	19.87 ± 3.75			

^aThe P_{app} values in the A to B (A-B) or B to A (B-A) were calculated by the following formula: P_{app}=(V_A/(Area×Time))×([drug]_{acceptor}/[drug]_{initial donor}) where, V_A=the volume in the acceptor well (in this assay: 0.3 or 1.0 mL), Area=the surface area of the

membrane (in this assay: 0.33 cm²), Time=the total transport time in seconds (in this assay: 5400 s), P_{app} values are expressed as 10⁻⁶ cm/s.

^bHuman absorbed fraction (F_{abs}).

^cThe B-A/A-B ratio was calculated by dividing the Papp values from B to A by the Papp values from A to B as follows. Efflux ratio (B-A/A-B ratio) = P_{app} (B to A) / P_{app} (A to B)

^d F_{abs} % > 70%, high permeability; 30% < F_{abs} % < 70%, moderate permeability; F_{abs} % < 30%, poor permeability.

Selectivity and Safety Profiles of Compound 16. Prior to evaluate in vivo efficiency, selectivity study of compound **16** against other PDE isoforms and dopamine receptor D1/D2 which are potential targets of berberine were performed.²⁶ The data in Table 4 reveal that **16** is highly selective for PDE4D vs PDE1, 2, 5-9, and PDE11 and exhibits at least 4-fold selectivity over PDE3 and PDE10. As shown in Figure S7, compound **16** is neither an agonist nor an antagonist for dopamine receptor D1/D2. Moreover, we tested hERG (the human Ether-à-go-go-Related Gene) inhibition effect of **16** using QPatch of automated patch clamping measurement (Figure S8).²⁷ It inhibits hERG with an IC₅₀ value over 40 μM, much weaker than that of a real hERG inhibitor (cisapride, IC₅₀: 0.07 μM). These data indicate that **16** is a PDE4 selective inhibitor without the inhibition to dopamine receptors or hERG.

Table 4. Selectivity of Compound 16 to 11 PDE Enzymes

PDEs	IC ₅₀ (μM)	Selectivity Index
------	-----------------------	-------------------

PDE1A ^a	>50	>200
PDE2A ^a	>50	>200
PDE3A ^a	56.6% @ 1 μ M	-
PDE4D ^b	0.24 \pm 0.01	-
PDE5A ^b	>5	>20
PDE6C ^a	3.3 \pm 0.03	13
PDE7A ^b	>5	>20
PDE8A1 ^a	>50	>200
PDE9A ^b	>50	>200
PDE10A ^b	0.92 \pm 0.07	4
PDE11A4 ^a	>50	>200

^aCommercial recombinant human full length PDEs (BPS Bioscience Inc. U.S.).

^bRecombinant human PDE catalytic domain prepared in our laboratory.

Pharmacokinetic Profiles of 16. A preliminary pharmacokinetic assessment was performed on **16** and the results were summarized in Table 5. Six male Sprague-Dawley rats were randomly divided into two groups. After oral administration of a 25 mg/kg dose of **16** to a group of three SD rats, it revealed a T_{max} of 1.33 h, $t_{1/2}$ of 0.94 h and a good oral bioavailability of 68.3%. The same experiment with intravenous administration of **16** at a dose of 10 mg/kg revealed a moderate plasma clearance (CL = 1.70 L/h/kg), but a much smaller volume of distribution and a shorter $t_{1/2}$.

Table 5. Pharmacokinetic Data of Compound 16 in Rats

route	T_{max} (h)	C_{max} (ng/mL)	AUC _{0-t} (ng·h/mL)	AUC _{0-∞} (ng·h/mL)	MRT (h)	$t_{1/2}$ (h)	CL (L/h/kg)	V_{ss} (L/kg)	F (%)
IV (10 mg/kg)	/	/	6213 \pm 1750	6276 \pm 1769	0.92 \pm 0.05	0.60 \pm 0.07	1.70 \pm 0.46	1.56 \pm 0.51	/
PO (25 mg/kg)	1.33 \pm 0.58	2447 \pm 703	8388 \pm 2201	8458 \pm 2232	2.50 \pm 0.10	0.94 \pm 0.20	/	/	68.3

In Vivo Efficacy of Compound 16. We further examined anti-inflammatory effects of **16** in animal models. Using apremilast as a positive control, the LPS-induced murine acute inflammation model was tested at first.²⁸ The compound was given 1.5 h prior to LPS injection, and concentrations of TNF- α , IL-6, IL-10, and IL-12p40 in serum and spleen were measured 2 h after the LPS treatment. LPS significantly increased the level of inflammatory cytokines in the serum and spleen in vehicle mice, while oral administration of **16** (1 mg/kg) prominently down-regulated the secretion of inflammatory cytokines, such as TNF- α , IL-6 and IL-12p40 (Figure 5). The results indicate that compound **16** is able to effectively attenuate inflammation and is promising for the treatment of inflammatory diseases.

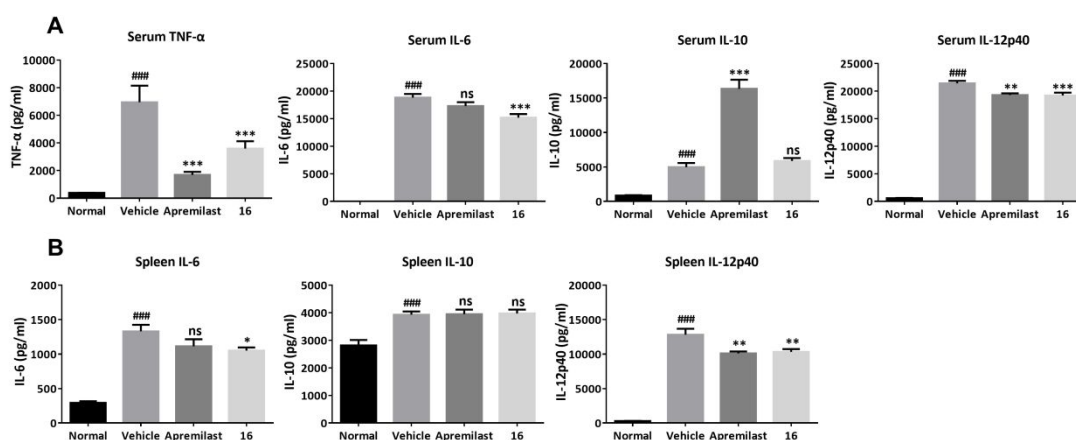
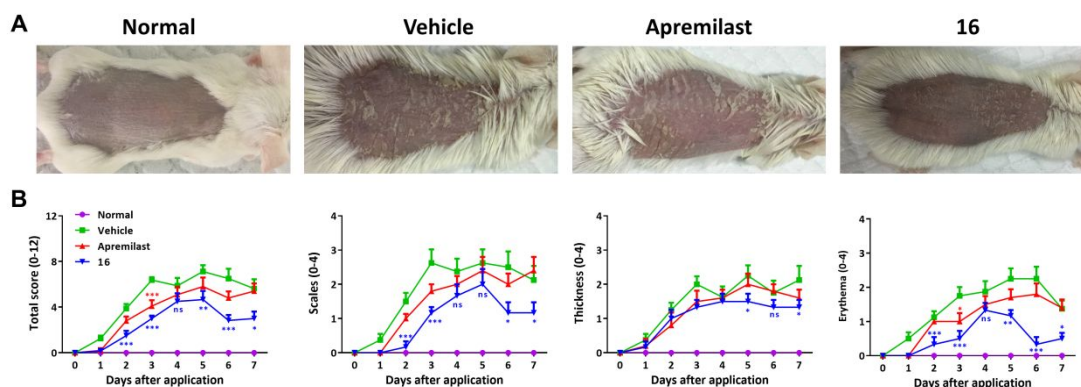


Figure 5. (A) Histograms representation of inflammation cytokines concentrations in serum of LPS-induced mice model after an oral administration of compound **16** (1 mg/kg) or apremilast (1 mg/kg) only once at 1.5 h before LPS application (n=6, female). (B) Similar inflammation cytokines concentration profiles in spleen at the same dose are displayed (n=6). Data are given as mean \pm S.E.M. Statistical analysis is performed

by one-way ANOVA. * $P < 0.05$, ** $P < 0.01$ and *** $P < 0.001$ compared with vehicle.

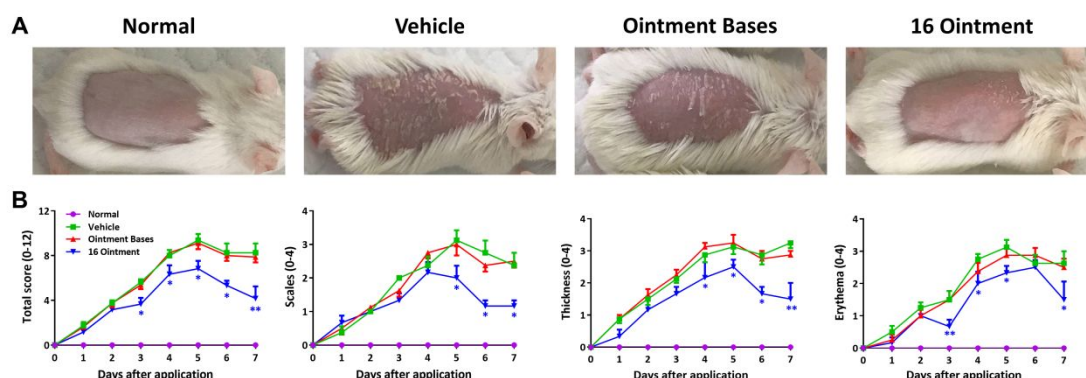
$P < 0.05$, ## $P < 0.01$ and ### $P < 0.001$ compared with normal.

Owing to the effects of imiquimod (IMQ) on the development of psoriasis-like skin inflammation, topical application of IMQ-containing cream to the skin of mice is a typical model for mimicking the clinical symptoms of patients with psoriasis.^{29,30} Encouraged by a good suppressive effect of **16** in LPS-induced inflammation, we further investigated efficacy of the compound in the IMQ-induced murine psoriasis model. Daily application of IMQ-containing cream at a dose of 62.5 mg on BALB/c mice for 7 days, severe lesions with thick scales and erythema appeared on the back skin. Strikingly, as shown in Figure 6, an oral administration of **16** with a dose of 25 mg/kg significantly attenuates the clinical features of skin lesions. It even shows much better therapeutic efficacy than apremilast at the same dose (25 mg/kg) both in individual scores for scales, thickness and erythema, and in the cumulative score (Figure 6). These results demonstrate that compound **16** is capable of effective preventing the IMQ-induced psoriasis-like skin lesions in mice and provides a good candidate for the development of a new anti-psoriasis drug.



1
2
3
4 **Figure 6.** Efficacy of oral administration of **16** or apremilast at a dose of 25 mg/kg once
5
6
7 daily to the IMQ-induced psoriasis-like mice. (A) A representative phenotypic
8
9 manifestation of back skin in each group (n=6, female) after IMQ treatment for 7 days.
10
11
12 (B) The cumulative scores were monitored daily ranging from 0 to 12, including scales,
13
14 thickness and erythema. Data are given as mean \pm SEM. *P < 0.05, **P < 0.01 and
15
16 ***P < 0.001, compared with vehicle.

17
18
19
20
21
22 **Efficacy of Topical Treatment with Compound 16.** Local medication is more
23
24 convenient and usually less in side effects for psoriasis patients. Therefore, we further
25
26 tested therapeutic effects of a topical application of compound **16** in the IMQ-induced
27
28 psoriasis-like mice model. The same experiment setup was used to generate the IMQ-
29
30 applied mice but they were treated daily with ointment bases or a topical cream
31
32 containing 2% of compound **16** at the same dose as that of the IMQ cream (62.5 mg per
33
34 day). The topical application of compound **16** yielded a significant therapeutic efficacy
35
36 in the IMQ-induced skin inflammation, manifesting with scales, thickness, and
37
38 erythema, similar to those were resulted from the oral administration of **16** (Figures 6
39
40 and 7).
41
42
43
44
45
46
47



1
2
3
4 **Figure 7.** The therapeutic efficacy of a topical application of compound **16** in the IMQ-
5
6 induced psoriasis-like mice. The cream with or without 2% of compound **16** at a dose
7
8 of 62.5 mg once daily were topically applied to the back skin of the mice. (A) A
9
10 representative phenotypic manifestation of back skin in each group (n=6, female)
11
12 during 7 days of treatment with or without **16**. (B) The cumulative scores were
13
14 monitored daily ranging from 0 to 12, including scales, thickness and erythema. Data
15
16 are given as mean \pm SEM. *P < 0.05, **P < 0.01 and ***P < 0.001, compared with
17
18 vehicle.
19
20
21
22
23
24
25
26

27 CONCLUSIONS

28
29
30
31 Given the effectiveness of PDE4 as a pivotal target for numerous inflammatory
32
33 diseases, both in academia and pharmaceutical industry there is continuing interest in
34
35 the discovery of novel PDE4 inhibitors with minimal side effects. Here, we reported
36
37 the discovery of novel PDE4 inhibitors with minimal side effects. Here, we reported
38
39 the structure-aided identification of a hit compound with a tetrahydro-isoquinoline
40
41 scaffold as a novel inhibitor of PDE4 after the screening of a berberine-like analogue
42
43 library. The determination of multiple protein-ligand structures in conjunction with the
44
45 ligand binding thermodynamic signature leads us to rapidly gain sufficient knowledge
46
47 on the binding mode as well as SAR of the tetrahydro-isoquinolines acting on PDE4D.
48
49 Small modification on this scaffold results in the discovery of compound **16** as a potent
50
51 PDE4 inhibitor both at the enzymatic level and in inhibition of the TNF- α production
52
53 in hPBMC. Moreover, the compound has a perfect cell-penetrating ability, a good
54
55
56
57
58
59
60

1
2
3
4 selectivity to PDE4 over other PDEs in most cases, and a good safety reflected in
5
6 extremely low inhibition of hERG or dopamine receptor D1/D2 which are potential
7
8 targets of berberine. Most importantly, **16** exhibits a significant effect on preventing
9
10 LPS-induced acute inflammation and IMQ-induced psoriasis-like skin lesions in mice,
11
12 providing a preclinical proof for the topical application of tetrahydro-isoquinolines as
13
14 an effective treatment strategy in psoriasis.
15
16
17
18
19
20

21 **EXPERIMENTAL SECTION**

22
23
24
25 **Chemistry. General Information.** The reagents (chemicals) were purchased from
26
27 commercial chemical reagent company, and used without further purification unless
28
29 otherwise stated. Analytical thin-layer chromatography (TLC) is HSGF 254. All
30
31 products were characterized by their NMR and HRMS spectra. The purity of tested
32
33 compounds was determined by HPLC (Agilent Eclipse XBD-C18, 5 μ m, 4.6*150 mm,
34
35 30 $^{\circ}$ C, UV 214/230/238/254 nm, flow rate = 1.0 mL/min) with aqueous CH₃CN or
36
37 CH₃OH (50%-70%) for 15 min. All compounds used for crystal structures
38
39 determination and functional studies possess \geq 95% purity (Table S4). Chemical shifts
40
41 were reported in parts per million (ppm, δ) downfield from tetramethylsilane. Proton
42
43 coupling patterns are described as singlet (s), doublet (d), triplet (t), quartet (q), multipet
44
45 (m), and broad (br).
46
47
48
49
50
51
52
53
54
55
56
57
58
59
60

1
2
3
4 The preparation of compounds **1-21** is described below while the chemistry
5
6 experimental procedure of key intermediates (**3a-7a**) is provided in Supporting
7
8 Information.
9
10

11
12
13 **(±)-1-(2-(1*H*-indol-3-yl)ethyl)-6,7-dimethoxy-3,4-dihydroisoquinoline-2(1*H*)-**
14
15 **methanal (1).** To a solution of **5a** (1.98 g, 5.325 mmol) in ethyl formate (20 mL) was
16
17 added trimethylamine (catalytic amount, 0.054 g). The mixture was stirred at 50 °C for
18
19 12 h. The reaction mixture was extracted with ethyl acetate. The organic layer was
20
21 washed with brine, dried over Na₂SO₄, filtered and concentrated under vacuum. The
22
23 residue was purified by the column chromatography (petroleum ether/ethyl acetate=1:1)
24
25 to afford the compound **1** (1.55 g, 80%) as a white solid. ¹H NMR (500 MHz, CDCl₃):
26
27 δ 8.32, 8.24 (2 × brs, 1H), 8.14, 8.07 (2 × brs, 1H), 7.63-7.56 (m, 1H), 7.43-7.34 (m,
28
29 1H), 7.25 – 7.02 (m, 3H), 6.59, 6.57 (2 × s, 1H), 6.43, 6.42 (2 × s, 1H), 5.51-5.45, 4.60
30
31 – 4.53 (2 × m, 1H), 4.50 – 4.42, 3.80-3.70 (2 × m, 1H), 3.87, 3.86(2 × s, 3H), 3.76, 3.70
32
33 (2 × s, 3H), 3.70-3.55, 3.19-3.11 (2 × m, 1H), 3.01 – 2.68 (m, 4H), 2.36-2.20 (m, 2H).
34
35 ¹³C NMR (125 MHz, CDCl₃): δ 161.98, 161.83, 148.07, 147.86, 147.67, 136.69,
36
37 136.46, 128.79, 128.77, 127.29, 127.08, 125.66, 124.57, 122.26, 121.98, 121.91,
38
39 121.84, 119.45, 119.18, 118.83, 118.75, 115.49, 114.45, 111.60, 111.42, 111.34,
40
41 111.18, 110.03, 109.60, 56.16, 56.01, 55.91, 55.88, 50.47, 40.35, 36.95, 36.25, 34.30,
42
43 29.41, 27.56, 22.29, 22.13. HRMS (ESI): exact mass calculated for C₂₂H₂₅N₂O₃⁺
44
45 [M+H]⁺:365.1787, found.365.1857.
46
47
48
49
50
51
52
53
54
55
56
57
58
59
60

1
2
3
4 **(S)-1-(2-(1*H*-indol-3-yl)ethyl)-6,7-dimethoxy-3,4-dihydroisoquinoline-2(1*H*)-**
5
6
7 **methanal (2).** This compound (a white solid) was prepared by replacement of **5a** with
8
9 **6a** using a similar synthetic procedure of product **1**. **¹H NMR** (400 MHz, CDCl₃): δ
10 8.29, 8.21 (2 × s, 1H), 8.13, 8.06 (2 × brs, 1H), 7.67-7.55 (m, 1H), 7.41-7.34 (m, 1H),
11
12 7.24 – 7.06 (m, 3H), 6.57, 6.55 (2 × s, 1H), 6.41, 6.39 (2 × s, 1H), 5.50-5.43, 4.59-4.51
13
14 (2 × m, 1H), 4.47-4.40, 3.78-3.72 (2 × m, 1H), 3.84, 3.83 (2 × s, 3H), 3.74, 3.68 (2 × s,
15
16 3H), 3.67-3.58, 3.18-3.07 (2 × m, 1H), 3.02 – 2.63 (m, 4H), 2.36 – 2.17 (m, 2H). **¹³C**
17
18 **NMR** (125 MHz, CDCl₃): δ 161.81, 161.68, 148.06, 147.83, 147.66, 136.68, 136.46,
19
20 128.81, 127.29, 127.08, 125.68, 124.58, 122.26, 121.95, 121.91, 121.79, 119.45,
21
22 119.18, 118.83, 118.74, 115.51, 114.47, 111.59, 111.41, 111.34, 111.18, 110.02,
23
24 109.56, 56.11, 55.99, 55.91, 55.87, 50.44, 40.27, 36.95, 36.26, 34.26, 29.39, 27.56,
25
26 22.28, 22.10. HRMS (ESI): exact mass calculated for C₂₂H₂₅N₂O₃⁺ [M+H]⁺: 365.1860,
27
28 found: 365.1861.
29
30
31
32
33
34
35
36
37
38
39
40

41 **(R)-1-(2-(1*H*-indol-3-yl)ethyl)-6,7-dimethoxy-3,4-dihydroisoquinoline-2(1*H*)-**
42
43 **methanal (3).** This compound (a white solid) was prepared by replacement of **5a** with
44
45 **7a** using a similar synthetic procedure of product **1**. **¹H NMR** (500 MHz, CDCl₃): δ
46 8.32 (brs, 1H), 8.23 (brs, 1H), 7.68-7.56 (m, 1H), 7.43-7.34 (m, 1H), 7.25 – 7.00 (m,
47
48 3H), 6.59, 6.57 (2 × s, 1H), 6.43, 6.42 (2 × s, 1H), 5.53-5.46, 4.62 – 4.53 (2 × m, 1H),
49
50 4.50 – 4.40, 3.80-3.70 (2 × m, 1H), 3.86, 3.85(2 × s, 3H), 3.76, 3.70 (2 × s, 3H), 370-
51
52 3.60, 3.22-3.09 (2 × m, 1H), 3.02 – 2.66 (m, 4H), 2.38-2.16(m, 2H). **¹³C NMR** (125
53
54 MHz, CDCl₃): δ 162.04, 161.88, 148.07, 147.86, 147.84, 147.67, 136.73, 136.50,
55
56
57
58
59
60

26

1
2
3
4 128.81, 128.76, 127.28, 127.08, 125.65, 124.59, 122.19, 122.07, 121.96, 121.86,
5
6
7 119.38, 119.13, 118.80, 118.72, 115.37, 114.29, 111.61, 111.49, 111.37, 111.24,
8
9 110.04, 109.63, 56.18, 56.02, 55.92, 55.88, 50.51, 40.38, 36.98, 36.25, 34.33, 29.42,
10
11 27.56, 22.30, 22.15. HRMS (ESI): exact mass calculated for $C_{22}H_{25}N_2O_3^+$ $[M+H]^+$:
12
13 365.1860, found: 365.1862.
14
15
16
17
18

19 **6,7-dimethoxy-3,4-dihydroisoquinoline-2(1H)-carbaldehyde (4)**. To a solution of
20
21 formic acid (20 mL), was slowly added compound **1a** (1.81 g, 10 mmol) at 0 °C for 10
22
23 min, then polyformaldehyde (1.8 g, 12 mmol) was added. The mixture was stirred at
24
25 50 °C for 12 h. The reaction mixture was cooled to room temperature, and alkalinized
26
27 pH to 9 by 1 M NaOH. The mixture was quenched with water and extracted with
28
29 dichloromethane, washed with brine, dried over Na_2SO_4 , filtered and concentrated. The
30
31 residue was dissolved in ethyl formate (20 mL), added trimethylamine (catalytic
32
33 amount, 0.101 g). The mixture was stirred at 50 °C for 12 h. The reaction mixture was
34
35 extracted with ethyl acetate. The organic layer was washed with brine, dried over
36
37 Na_2SO_4 , filtered and concentrated under vacuum. The residue was purified by the
38
39 column chromatography (petroleum ether/ethyl acetate=1:1) to afford the titled
40
41 compound **4** (1.76 g, 80%) as a white solid. 1H NMR (400 MHz, $CDCl_3$): δ 8.25, δ 8.19
42
43 (2 × s, 1H), 6.62, 6.60 (2 × s, 1H), 6.60, 6.57 (2 × s, 1H), 4.61, 4.48 (2 × s, 2H), 3.86
44
45 (s, 6H), 3.78, 3.63 (2 × t, J = 6.0 Hz, 2H), 2.88 – 2.74 (m, 2H). ^{13}C NMR (125 MHz,
46
47 $CDCl_3$): δ 161.60, 161.14, 148.12, 148.10, 147.83, 147.82, 126.33, 125.35, 123.91,
48
49 123.64, 111.82, 111.54, 109.20, 108.67, 56.03, 55.99, 55.96, 47.09, 43.40, 41.98, 38.04,
50
51
52
53
54
55
56
57
58
59
60

27

29.27, 27.54. HRMS (ESI): exact mass calculated for $C_{12}H_{16}NO_3^+$ $[M+H]^+$: 222.1052 ,
found: 222.1123 .

7-ethoxy-6-methoxy-3,4-dihydroisoquinoline-2(1H)-carbaldehyde (5). This compound (a white solid) was prepared by replacement of **1a** with **1b** using a similar synthetic procedure of product **4**. **1H NMR** (600 MHz, $CDCl_3$): δ 8.27, 8.21 (2 \times s, 1H), 6.64, 6.62 (2 \times s, 1H), 6.61, 6.60 (2 \times s, 1H), 4.62, 4.48 (2 \times s, 2H), 4.08 (q, J = 7.0 Hz, 2H), 3.87, 3.86 (2 \times s, 3H), 3.80, 3.65 (2 \times t, J = 6.0 Hz, 2H), 2.84, 2.81 (2 \times t, J = 6.0 Hz, 2H), 1.52 – 1.44 (m, 3H). **^{13}C NMR** (150 MHz, $CDCl_3$): δ 161.59, 161.13, 148.45, 148.12, 147.38, 147.12, 126.35, 125.33, 123.86, 123.59, 112.05, 111.77, 110.64, 110.19, 64.56, 64.46, 56.01, 47.07, 43.41, 41.96, 38.04, 29.27, 27.55, 14.81, 14.76. HRMS (ESI): exact mass calculated for $C_{13}H_{18}NO_3^+$ $[M+H]^+$: 236.1281, found: 236.1277.

6-ethoxy-7-methoxy-3,4-dihydroisoquinoline-2(1H)-carbaldehyde (6). This compound (a white solid) was prepared by replacement of **1a** with **1c** using a similar synthetic procedure of product **4**. **1H NMR** (600 MHz, $CDCl_3$): δ 8.24, 8.18 (2 \times s, 1H), 6.62, 6.59 (2 \times s, 1H), 6.59, 6.57 (2 \times s, 1H), 4.60, 4.46 (2 \times s, 2H), 4.09-4.02 (m, 2H), 3.84, 3.83 (2 \times s, 3H), 3.77, 3.62 (2 \times t, J = 6.0 Hz, 2H), 2.81, 2.77 (2 \times t, J = 6.06.0 Hz, 2H), 1.48-1.42 (m, 3H). **^{13}C NMR** (150 MHz, $CDCl_3$): δ 161.59, 161.14, 148.40, 148.12, 147.43, 147.12, 126.29, 125.30, 123.88, 123.64, 113.24, 113.03, 109.44, 108.91, 64.44, 64.42, 56.09, 56.05, 47.10, 43.42, 41.99, 38.05, 29.25, 27.52, 14.80,

1
2
3
4 14.78. HRMS (ESI): exact mass calculated for $C_{13}H_{17}NO_3^+$ $[M+H]^+$: 236.1281, found:
5
6 236.1282.
7
8
9

10
11 **(S)-1-((1*H*-indol-3-yl)methyl)-6,7-dimethoxy-3,4-dihydroisoquinoline-2(1*H*)-**
12
13 **methanal (7)**. This compound (a white solid) was prepared by replacement of **5a** with
14 **6b** using a similar synthetic procedure of product **1**. **1H NMR** (400 MHz, $CDCl_3$): δ
15 8.37, 8.21 (2 \times s, 1H), 8.15, 7.57 (2 \times s, 1H), 7.67-7.53 (m, 1H), 7.41-7.30 (m, 1H),
16 7.25-7.04 (m, 2H), 6.96-6.87 (m, 1H), 6.68, 6.55 (2 \times s, 1H), 6.64, 6.31 (2 \times s, 1H),
17 5.71-5.61, 4.76-4.64 (2 \times m, 1H), 4.54-4.44, 3.61-3.54 (2 \times m, 1H), 3.88, 3.84 (2 \times s,
18 3H), 3.86, 3.55 (2 \times s, 3H), 3.45 – 3.10 (m, 3H), 2.96 – 2.62 (m, 2H). **^{13}C NMR** (125
19 MHz, $CDCl_3$): δ 161.56, 161.51, 148.30, 147.84, 147.67, 147.31, 136.44, 136.06,
20 127.91, 127.87, 127.80, 126.85, 126.12, 125.19, 123.59, 123.00, 122.39, 122.07,
21 119.80, 119.64, 119.09, 118.13, 112.05, 111.65, 111.42, 111.22, 110.98, 110.58,
22 110.03, 57.44, 56.12, 55.95, 55.88, 55.63, 51.20, 40.82, 33.94, 33.34, 31.80, 29.22,
23 27.79. HRMS (ESI): exact mass calculated for $C_{21}H_{23}N_2O_3^+$ $[M+H]^+$: 351.1703, found:
24
25 351.1704.
26
27
28
29
30
31
32
33
34
35
36
37
38
39
40
41
42
43
44
45
46
47

48 **(S)-1-(3-(1*H*-indol-3-yl)propyl)-6,7-dimethoxy-3,4-dihydroisoquinoline-**
49
50 **2(1*H*)-carbaldehyde (8)**. This compound (a white solid) was prepared by replacement
51 of **5a** with **6c** using a similar synthetic procedure of product **1**. **1H NMR** (400 MHz,
52 DMSO): δ 10.87, 10.74 (2 \times s, 1H), 8.18, 8.15 (2 \times s, 1H), 7.43-7.23 (m, 2H), 7.08-
53 6.90 (m, 2H), 6.82-6.72 (m, 1H), 6.64-6.52 (m, 2H), 5.55-5.46, 5.06-4.95 (2 \times m, 1H),
54
55
56
57
58
59
60

1
2
3
4 3.73-3.63, 3.41-3.24 (2 × m, 1H), 3.65 (s, 3H), 3.58, 3.54 (2 × s, 3H), 3.22-3.10, 3.09-
5
6 2.94 (2 ×m, 1H), 2.81-2.57 (m, 4H), 2.08-1.71 (m, 4H). ¹³C NMR (125 MHz, DMSO):
7
8
9 δ 164.12, 163.42, 149.16, 147.79, 147.74, 136.80, 136.59, 132.55, 132.22, 132.18,
10
11 131.46, 127.26, 127.11, 121.80, 121.52, 121.09, 120.74, 118.87, 118.78, 118.49,
12
13 118.32, 113.02, 112.90, 112.69, 112.45, 112.33, 112.32, 111.68, 111.54, 55.98, 55.94,
14
15 55.72, 55.70, 53.13, 47.47, 47.17, 44.46, 37.21, 34.35, 30.72, 28.94, 22.58, 22.21, 20.85.
16
17
18
19
20 HRMS (ESI): exact mass calculated for C₂₃H₂₆N₂O₃⁺ [M+H]⁺: 379.2016, found:
21
22 379.2027.
23
24
25
26

27 **(±)-(1-(2-(1*H*-indol-3-yl)ethyl)-6,7-dimethoxy-3,4-dihydroisoquinoline-2(1*H*-**
28
29 **yl)(pyridin-4-yl)methanone (9)**. To a solution of isonicotinic acid (37 mg, 0.297
30
31 mmol) in CH₂Cl₂ was added HOBt (1-hydroxybenzotriazole, 47 mg, 0.356 mmol),
32
33 EDC-HCl (1-ethyl-3-(3-dimethylaminopropyl) carbodiimide hydrochloride, 69 mg,
34
35 0.356 mmol), **5a** (100 mg, 0.297 mmol), and TEA (triethylamine, 0.084 mL, 0.588
36
37 mmol). The mixture was stirred for 12 h at room temperature, washed with water and
38
39 brine, dried over Na₂SO₄, filtered and concentrated under vacuum. The residue was
40
41 purified by the column chromatography (petroleum ether/ethyl acetate=1:1) to afford
42
43 the corresponding product **9** as a white solid. ¹H NMR (400 MHz, CDCl₃): δ 8.72,
44
45 8.56 (2 × d, *J* = 5.7, 4.5 Hz, 2H), 8.14, 8.06 (2 × brs, 1H), 7.61, 7.49 (d, *J* = 7.8,
46
47 7.9 Hz, 1H), 7.40 – 7.32 (m, 1H), 7.31 – 7.08 (m, 4H), 6.65 (s, 1H), 6.60, 6.56 (s,
48
49 1H), 6.48, 6.23 (2 × s, 1H), 5.81 – 4.64 (m, 1H), 3.87, 3.84 (2 × s, 3H), 3.75 – 3.62
50
51 (m, 3H), 3.61 – 3.35 (m, 1H), 3.16 – 2.74 (m, 3H), 2.71 – 2.57 (m, 1H), 2.47 –
52
53
54
55
56
57
58
59
60

30

1
2
3
4 2.36 (m, 1H), 2.35 – 2.23 (m, 1H), 2.20 – 2.10 (m, 1H). ¹³C NMR (125 MHz,
5
6 CDCl₃): δ 168.32, 168.21, 150.42, 150.16, 148.29, 147.91, 147.56, 144.36, 144.14,
7
8
9 136.48, 129.20, 128.59, 127.29, 125.61, 124.32, 122.33, 122.04, 121.90, 121.21,
10
11
12 120.79, 119.50, 119.31, 118.72, 118.56, 115.42, 114.61, 111.81, 111.32, 111.23,
13
14
15 110.18, 109.37, 57.30, 55.94, 55.89, 51.87, 41.15, 37.22, 36.91, 35.92, 29.71, 28.89,
16
17 27.52, 22.35, 22.20. HRMS (ESI): exact mass calculated for C₂₇H₂₈N₃O₃⁺ [M+H]⁺
18
19 442.2125, found 442.2132.
20
21
22
23

24
25 **(±)-(1-(2-(1*H*-indol-3-yl)ethyl)-6,7-dimethoxy-3,4-dihydroisoquinolin-**
26
27 **2(1*H*-yl)(tetrahydro-2*H*-pyran-4-yl)methanone (10).** To a solution of 5a (100
28
29 mg, 0.297 mmol) in CH₂Cl₂ (20 mL) was added trimethylamine (catalytic amount,
30
31 0.054 g) and then the mixture was added tetrahydro-2*H*-pyran-4-carbonyl chloride
32
33 slowly in 0 °C. The mixture was stirred at room temperature for 2 h. The reaction
34
35 mixture was extracted with ethyl acetate. The organic layer was washed with brine,
36
37 dried over Na₂SO₄, filtered and concentrated under vacuum. The residue was
38
39 purified by the column chromatography (petroleum ether/ethyl acetate=1:1) to
40
41 afford the compound **10** as a white solid. ¹H NMR (500 MHz, CDCl₃): δ 8.14, 8.01
42
43 (2 × s, 1H) , 7.58, 7.53 (2 × s, 1H), 7.40, 7.35 (2 × d, *J* = 8.1, 8.0 Hz, 1H), 7.24 – 7.06
44
45 (m, 3H), 6.63 – 6.42 (m, 2H), 5.77-5.69, 4.85-4.79 (2 × m, 1H), 4.67-4.59, 3.98-3.91 (2
46
47 × m, 1H), 4.06 (d, *J* = 8.0 Hz, 1H), 3.88 – 3.78 (m, 4H), 3.67 – 3.61 (m, 2H), 3.56 –
48
49 3.42 (m, 1H), 3.23 – 2.98 (m, 1H), 2.97 – 2.71 (m, 4H), 2.70 – 2.41 (m, 2H), 2.36 –
50
51
52
53
54
55
56
57
58
59
60

1
2
3
4 1.94 (m, 4H), 1.73 (d, $J = 13.5$ Hz, 1H), 1.65 – 1.55 (m, 2H). ^{13}C NMR (125 MHz,
5
6
7 CDCl_3): δ 173.73, 173.34, 148.16, 147.67, 147.42, 136.59, 136.40, 130.07, 129.21,
8
9 127.35, 127.25, 126.69, 124.79, 122.53, 121.91, 121.72, 120.99, 119.63, 119.16,
10
11 118.71, 115.73, 115.04, 111.86, 111.42, 111.12, 111.09, 110.43, 109.86, 67.38, 67.34,
12
13 67.19, 67.01, 56.23, 55.94, 55.90, 55.86, 54.93, 51.78, 39.64, 38.24, 37.97, 36.84, 36.70,
14
15 35.87, 29.75, 29.62, 29.19, 28.99, 28.58, 27.61, 22.08, 21.94. HRMS (ESI): exact mass
16
17
18 calculated for $\text{C}_{27}\text{H}_{33}\text{N}_2\text{O}_4^+$ $[\text{M}+\text{H}]^+$ 449.2435, found 449.2438.
19
20
21
22
23

24 **(±)-1-(2-(1*H*-indol-3-yl)ethyl)-6,7-dimethoxy-2-((tetrahydro-2*H*-pyran-4-**
25 **yl)methyl)-1,2,3,4-tetrahydroisoquinoline (11).** To a solution of **5a** (100 mg, 0.297
26
27 mmol) in acetonitrile (20 mL) was added potassium carbonate, 4-
28
29 (bromomethyl)tetrahydro-2*H*-pyran. The mixture was refluxed overnight. The reaction
30
31 mixture was extracted with ethyl acetate. The organic layer was washed with brine,
32
33 dried over Na_2SO_4 , filtered and concentrated under vacuum. The residue was purified
34
35 by the column chromatography (petroleum ether/ethyl acetate=1:1) to afford the
36
37 compound **11** as a white solid. ^1H NMR (400 MHz, CDCl_3): δ 7.98 (brs, 1H), 7.59
38
39 (d, $J = 7.8$ Hz, 1H), 7.36 (d, $J = 8.1$ Hz, 1H), 7.18 (t, $J = 7.1$ Hz, 1H), 7.11 (dd, J
40
41 = 11.0, 3.9 Hz, 1H), 6.99 (s, 1H), 6.56 (s, 1H), 6.46 (s, 1H), 3.98 (dd, $J = 11.4$, 2.9
42
43 Hz, 2H), 3.84 (s, 3H), 3.76 (s, 3H), 3.63 – 3.47 (m, 1H), 3.38 (td, $J = 10.9$, 3.3 Hz,
44
45 2H), 3.31 – 3.16 (m, 1H), 3.05 – 2.67 (m, 4H), 2.60 – 2.30 (m, 3H), 2.24 – 1.96
46
47 (m, 2H), 1.88 – 1.67 (m, 3H), 1.28 (m, 2H). ^{13}C NMR (125 MHz, CDCl_3): δ 147.23,
48
49 136.49, 130.93, 127.56, 126.60, 121.96, 121.01, 119.12, 118.98, 116.97, 111.40,
50
51
52
53
54
55
56
57
58
59
60

32

1
2
3
4 111.10, 110.67, 68.11, 61.35, 60.13, 55.89, 55.84, 43.98, 36.83, 33.79, 31.96, 31.74,
5
6
7 29.72, 23.66, 22.14. ESI-MS m/z 435.0 [M+H]⁺. HRMS (ESI): exact mass calculated
8
9 for C₂₇H₃₅N₂O₃⁺ [M+H]⁺ 435.2642, found 435.2654.

10
11
12
13 **(±)-1-(2-(1*H*-indol-3-yl)ethyl)-6,7-dimethoxy-2-(2,2,2-trifluoroethyl)-1,2,3,4-**
14
15
16 **tetrahydroisoquinoline (12).** This compound (a white solid) was prepared by
17
18 replacement of 4-(bromomethyl)tetrahydro-2*H*-pyran with 2-bromo-1,1,1-
19
20 trifluoroethane using a similar synthetic procedure of product **11**. **¹H NMR** (400 MHz,
21
22 CDCl₃): δ 7.94 (brs, 1H), 7.61 (d, J = 7.8 Hz, 1H), 7.36 (d, J = 8.1 Hz, 1H), 7.21
23
24 – 7.14 (m, 1H), 7.13 – 7.06 (m, 1H), 7.02 (s, 1H), 6.56 (s, 1H), 6.37 (s, 1H), 3.84
25
26 (s, 3H), 3.72 (s, 3H), 3.67 (dd, J = 8.4, 4.1 Hz, 1H), 3.43 – 3.31 (m, 1H), 3.24 (dq,
27
28 J = 15.4, 9.5 Hz, 1H), 3.11 – 2.81 (m, 5H), 2.52 (d, J = 14.7 Hz, 1H), 2.16 (dt, J
29
30 = 13.9, 7.0 Hz, 1H), 2.10 – 1.98 (m, 1H). **¹³C NMR** (125 MHz, CDCl₃): δ 147.55,
31
32 147.45, 136.50, 129.93, 127.51, 125.86, 121.90, 121.38, 119.12, 119.00, 116.64,
33
34 111.46, 111.08, 110.41, 62.74, 55.86, 55.70, 55.45, 55.21, 54.96, 44.55, 37.32, 29.72,
35
36 23.23, 21.87. HRMS (ESI): exact mass calculated for C₂₃H₂₆F₃N₂O₂⁺ [M+H]⁺
37
38 419.1941, found 419.1948.

39
40
41
42 **(±)-methyl-2-(1-(2-(1*H*-indol-3-yl)ethyl)-6,7-dimethoxy-3,4-**
43
44 **dihydroisoquinoline-2(1*H*)-yl)acetate (13).** This compound (a white solid) was
45
46 prepared by replacement of 4-(bromomethyl)tetrahydro-2*H*-pyran with methyl 2-
47
48 bromoacetate using a similar synthetic procedure of product **11**. **¹H NMR** (400 MHz,
49
50
51
52
53
54
55
56
57
58
59
60

1
2
3
4 CDCl₃): δ 7.97 (brs, 1H), 7.60 (d, $J = 7.9$ Hz, 1H), 7.35 (d, $J = 8.1$ Hz, 1H), 7.17 (ddd,
5
6
7 $J = 8.2, 7.2, 1.1$ Hz, 1H), 7.09 (ddd, $J = 7.9, 7.1, 1.0$ Hz, 1H), 7.04 (d, $J = 2.0$ Hz, 1H),
8
9
10 6.56 (s, 1H), 6.37 (s, 1H), 3.84 (s, 3H), 3.78 – 3.70 (m, 4H), 3.68 (s, 3H), 3.48 (dd, $J =$
11
12 39.3, 16.6 Hz, 2H), 3.34 (ddd, $J = 13.5, 9.8, 5.2$ Hz, 1H), 3.04 (dt, $J = 9.7, 5.2$ Hz, 1H),
13
14 3.00 – 2.87 (m, 2H), 2.82 (ddd, $J = 15.6, 9.7, 5.6$ Hz, 1H), 2.60 (dt, $J = 16.5, 4.5$ Hz,
15
16 1H), 2.27 – 2.15 (m, 1H), 2.14 – 2.03 (m, 1H). ¹³C NMR (125 MHz, CDCl₃): δ 172.05,
17
18 147.38, 136.46, 129.88, 127.56, 126.00, 121.86, 121.40, 119.08, 119.06, 116.81,
19
20 111.33, 111.05, 110.56, 60.54, 55.85, 55.80, 55.35, 51.65, 45.10, 36.77, 24.44, 21.73.
21
22
23
24
25
26 HRMS (ESI): exact mass calculated for C₂₄H₂₉N₂O₄⁺ [M+H]⁺ 409.2122, found
27
28 409.2118.
29
30
31

32
33 **(±)-1-(2-(1*H*-indol-3-yl)ethyl)-6,7-dimethoxy-2-(2-methoxyethyl)-1,2,3,4-**
34
35 **tetrahydroisoquinoline (14).** This compound (a white solid) was prepared by
36
37 replacement of 4-(bromomethyl)tetrahydro-2*H*-pyran with 1-bromo-2-methoxyethane
38
39 using a similar synthetic procedure of product **11**. ¹H NMR (400 MHz, CDCl₃): δ
40
41 8.06 (brs, 1H), 7.61 (d, $J = 7.9$ Hz, 1H), 7.36 (d, $J = 8.1$ Hz, 1H), 7.21 – 7.15 (m,
42
43 1H), 7.13 – 7.05 (m, 2H), 6.56 (s, 1H), 6.37 (s, 1H), 3.92-3.84 (m, 1H), 3.84 (s,
44
45 3H), 3.75 (s, 3H), 3.65 – 3.54 (m, 2H), 3.36 (s, 3H), 3.10- 2.76 (m, 7H), 2.63-2.51
46
47 (d, $J = 16.0$ Hz, 1H), 2.41-2.24 (m, 1H), 2.15 – 2.01 (m, 1H). ¹³C NMR (125 MHz,
48
49 CDCl₃): δ 147.37, 136.49, 127.56, 121.92, 121.54, 119.13, 118.99, 111.35, 111.12,
50
51 110.68, 60.94, 58.88, 55.85, 53.01, 44.40, 36.29, 29.71, 23.51, 22.18. HRMS (ESI):
52
53 exact mass calculated for C₂₄H₃₁N₂O₃⁺ [M+H]⁺ 395.2329, found 395.2336.
54
55
56
57
58
59
60

1
2
3
4 **(S)-1-(2-(6-fluoro-1*H*-indol-3-yl)ethyl)-6,7-dimethoxy-3,4-dihydroisoquinoline-**
5
6
7 **2(1*H*)-carbaldehyde (15).** This compound (a white solid) was prepared by replacement
8
9 of **5a** with **6d** using a similar synthetic procedure of product **2**. **¹H NMR** (400 MHz,
10 CDCl₃): δ 8.29, 8.20 (2 × s, 1H), 8.19, 8.11 (2 × brs, 1H), 7.55-7.42 (m, 1H), 7.14-6.98
11 (m, 2H), 6.95-6.81 (m, 1H), 6.58, 6.55 (2 × s, 1H), 6.41, 6.40 (2 × s, 1H), 5.48-5.42,
12 (m, 2H), 4.58-4.50 (2 × m, 1H), 4.48-4.38, 3.78-3.68 (2 × m, 1H), 3.84, 3.84 (2 × s, 3H), 3.77,
13
14
15
16
17
18
19
20
21
22
23
24
25
26
27
28
29
30
31
32
33
34
35
36
37
38
39
40
41
42
43
44
45
46
47
48
49
50
51
52
53
54
55
56
57
58
59
60
3.71 (2 × s, 3H), 3.67-3.57, 3.17-3.07(2 × m, 1H), 2.98-2.63 (m, 4H), 2.30-2.15 (m,
2H). **¹³C NMR** (125 MHz, CDCl₃): δ 161.86, 161.68, 161.04, 160.91, 159.14, 159.03,
148.13, 147.89, 147.87, 147.68, 136.66, 136.56, 136.41, 136.31, 128.67, 128.63,
125.72, 124.64, 123.92, 123.72, 122.20, 122.17, 122.01, 121.99, 119.48, 119.40,
119.32, 115.53, 114.55, 111.66, 111.39, 110.01, 109.55, 108.25, 108.05, 107.93,
107.74, 97.82, 97.61, 97.58, 97.37, 56.17, 56.01, 55.92, 55.88, 50.43, 40.28, 36.81,
36.18, 34.28, 29.36, 27.53, 22.19, 22.03. HRMS (ESI): exact mass calculated for
C₂₂H₂₄FN₂O₃⁺ [M+H]⁺: 383.1765, found: 383.1761.

43
44
45
46
47
48
49
50
51
52
53
54
55
56
57
58
59
60
(S)-6,7-dimethoxy-1-(2-(6-methyl-1*H*-indol-3-yl)ethyl)-3,4-
dihydroisoquinoline-2(1*H*)-carbaldehyde (16). This compound (a white solid) was
prepared by replacement of **5a** with **6e** using a similar synthetic procedure of product
2. **¹H NMR** (400 MHz, CDCl₃): δ 8.28, 8.19 (2 × s, 1H), 7.97, 7.89 (2 × brs, 1H), 7.55-
7.41 (m, 1H), 7.18, 7.15 (2 × s, 1H), 7.20-6.90 (m, 2H), 6.57, 6.55 (2 × s, 1H), 6.43,
6.40 (2 × s, 1H), 5.50-5.43, 4.59-4.51 (2 × m, 1H), 4.47-4.40, 3.78-3.70 (2 × m, 1H),
3.83 (2 × s, 3H), 3.75, 3.72 (2 × s, 3H), 3.66-3.58, 3.18-3.07 (2 × m, 1H), 2.98-2.64 (m,
35

1
2
3
4 4H), 2.46, 2.45 (2 × s, 3H), 2.33-2.17 (m, 2H). ¹³C NMR (125 MHz, DMSO): δ 162.38,
5
6 161.76, 148.06, 147.93, 147.82, 147.71, 137.33, 137.25, 130.36, 130.23, 129.63,
7
8 129.15, 125.80, 125.52, 125.48, 125.45, 122.16, 121.99, 120.44, 120.34, 118.44,
9
10 118.39, 114.30, 113.50, 112.51, 112.44, 111.71, 111.65, 111.02, 110.74, 56.01, 55.97,
11
12 55.94, 50.21, 39.59, 37.09, 36.57, 33.87, 29.25, 27.48, 22.42, 22.37, 21.85. HRMS
13
14 (ESI): exact mass calculated for C₂₃H₂₇N₂O₃⁺ [M+H]⁺: 379.2016, found: 379.2020.
15
16
17
18
19
20
21

22 **(S)-7-ethoxy-6-methoxy-1-(2-(6-methyl-1*H*-indol-3-yl)ethyl)-3,4-**
23
24 **dihydroisoquinoline-2(1*H*)-carbaldehyde (17).** This compound (a white solid)
25
26 was prepared by replacement of **5a** with **6f** using a similar synthetic procedure of
27
28 product **2**. ¹H NMR (500 MHz, CDCl₃): δ 8.27, 8.19 (2 × s, 1H), 7.96, 7.88 (2 × s,
29
30 1H), 7.50, 7.45 (2 × d, *J* = 8.1, 8.0 Hz, 1H), 7.18, 7.15 (2 × s, 1H), 7.05-6.92 (m, 2H),
31
32 6.57, 6.54 (2 × s, 1H), 6.41, 6.39 (2 × s, 1H), 5.48-5.42, 4.56-4.50 (2 × m, 1H), 4.43-
33
34 4.36, 3.75-3.67 (2 × m, 1H), 3.99-3.83 (m, 2H), 3.82 (s, 3H), 3.64-3.57, 3.15-3.07 ((2
35
36 × m, 1H), 2.96-2.64 (m, 4H), 2.47, 2.45 (2 × s, 3H), 2.29-2.15 (m, 2H), 1.40, 1.36 (2 ×
37
38 t, *J* = 7.0, 7.0 Hz, 3H). ¹³C NMR (150 MHz, CDCl₃): δ 161.79, 161.70, 148.33, 148.06,
39
40 147.08, 146.87, 137.13, 136.90, 132.05, 131.65, 128.79, 128.75, 125.65, 125.15,
41
42 124.94, 124.50, 121.20, 121.14, 120.91, 118.51, 118.43, 115.37, 114.27, 111.74,
43
44 111.49, 111.44, 111.33, 111.11, 64.50, 64.31, 56.03, 55.93, 50.43, 40.30, 36.99, 36.23,
45
46 34.25, 29.71, 29.39, 27.56, 22.32, 22.19, 21.69, 14.77, 14.69. HRMS (ESI): exact mass
47
48 calculated for C₂₄H₂₉N₂O₃⁺ [M+H]⁺: 393.2100, found 393.2175.
49
50
51
52
53
54
55
56
57
58
59
60

(S)-7-(cyclopropylmethoxy)-6-methoxy-1-(2-(6-methyl-1H-indol-3-yl)ethyl)-

3,4-dihydroisoquinoline-2(1H)-methanal (18). This compound (a white solid) was prepared by replacement of **5a** with **6g** using a similar synthetic procedure of product **2**. **¹H NMR** (400 MHz, CDCl₃): δ 8.27, 8.18 (2 × s, 1H), 7.97 (2 × brs, 1H), 7.50, 7.44 (d, *J* = 8.1, 8.0 Hz, 1H), 7.18, 7.15 (2 × s, 1H), 7.05 – 6.95 (m, 2H), 6.57, 6.55 (2 × s, 1H), 6.43, 6.40 (2 × s, 1H), 5.47-5.40, 4.58-4.47 (2 × m, 1H), 4.42-4.32, 3.89-3.81 (2 × m, 1H), 3.71 (s, 3H), 3.77-3.64 (m, 2H), 3.63-3.55, 3.16-3.05 (2 × m, 1H), 2.98 – 2.60 (m, 4H), 2.47, 2.45 (2 × s, 3H), 2.29-2.13 (m, 2H), 1.77-1.63 (m, 1H), 0.67-0.54 (m, 2H), 0.35-0.24 (m, 2H). **¹³C NMR** (125 MHz, CDCl₃): δ 161.77, 161.68, 153.18, 148.65, 148.36, 147.31, 147.09, 137.14, 136.90, 132.10, 131.69, 128.80, 128.73, 125.98, 125.18, 124.96, 124.82, 121.24, 121.17, 121.11, 120.94, 118.52, 118.41, 115.42, 114.34, 112.34, 112.07, 111.96, 111.73, 111.32, 111.10, 74.32, 74.07, 55.99, 50.40, 40.28, 36.86, 36.21, 34.24, 29.71, 29.41, 27.58, 22.30, 22.12, 21.69, 10.29, 10.23, 3.39, 3.31. HRMS (ESI): exact mass calculated for C₂₆H₃₁N₂O₃⁺ [M+H]⁺ 419.2256, found 419.2332.

(S)-7-(cyclopentyloxy)-6-methoxy-1-(2-(6-methyl-1H-indol-3-yl)ethyl)-3,4-

dihydroisoquinoline-2(1H)-methanal (19). This compound (a white solid) was prepared by replacement of **5a** with **6h** using a similar synthetic procedure of product **2**. **¹H NMR** (400 MHz, CDCl₃): δ 8.27, 8.19 (2 × s, 1H), 7.97, 7.89 (2 × brs, 1H), 7.51, 7.45 (2 × d, *J* = 8.0, 8.0 Hz, 1H), 7.18, 7.15 (2 × s, 1H), 7.06-6.86 (m, 2H), 6.56, 6.53 (2 × s, 1H), 6.40, 6.38 (2 × s, 1H), 5.48-5.39, 4.61-4.55 (2 × m, 1H), 4.55-

1
2
3
4 4.48 (m, 1H), 4.43-4.37, 3.75-3.68 (2 × m, 1H), 3.80 (s, 3H), 3.66-3.55, 3.16-3.05 (2 ×
5
6 m, 1H), 2.98 – 2.60 (m, 4H), 2.46, 2.45 (2 × s, 3H), 2.32-2.14 (m, 2H), 1.97-1.73 (m,
7
8 6H), 1.63-1.48 (m, 2H). ¹³C NMR (125 MHz, CDCl₃): δ 161.93, 161.86, 149.19,
9
10 148.91, 146.56, 146.34, 137.32, 137.07, 132.14, 131.74, 128.91, 128.84, 125.76,
11
12 125.29, 125.07, 124.59, 121.41, 121.35, 121.30, 121.01, 118.65, 118.56, 115.44,
13
14 114.34, 113.83, 113.51, 112.31, 112.11, 111.48, 111.25, 80.75, 80.54, 56.20, 56.17,
15
16 56.07, 50.55, 40.47, 37.08, 36.36, 34.41, 32.91, 32.82, 32.73, 29.83, 29.49, 27.69, 24.21,
17
18 24.18, 24.15, 22.45, 22.36, 21.81. HRMS (ESI): exact mass calculated for C
19
20 ₂₇H₃₃N₂O₃⁺ [M+H]⁺ 433.2413, found 433.2484.
21
22
23
24
25
26
27
28
29

30 **(S)-1-(2-(1*H*-indol-3-yl)ethyl)-7-ethoxy-6-methoxy-3,4-dihydroisoquinoline-**

31
32 **2(1*H*)-methanal (20).** This compound (a white solid) was prepared by replacement of
33
34 **5a** with **6i** using a similar synthetic procedure of product **2**. ¹H NMR (600 MHz,
35
36 CDCl₃): δ 8.28, 8.20 (2 × s, 1H), 8.13, 8.06 (2 × brs, 1H), 7.62, 7.57 (2 × d, J = 7.9 Hz,
37
38 1H), 7.39, 7.36 (2 × d, J = 8.1 Hz, 1H), 7.24-7.00 (m, 3H), 6.57, 6.54 (2 × s, 1H), 6.41,
39
40 6.40 (2 × s, 1H), 5.50-5.40, 4.60-4.50 (2 × m, 1H), 4.46-4.37, 3.76-3.68 (2 × m, 1H),
41
42 4.00-3.79 (m, 5H), 3.66-3.55, 3.17-3.08 (2 × m, 1H), 2.99-2.63 (m, 4H), 2.31-2.17 (m,
43
44 2H), 1.40, 1.36 (2 × t, J = 7.0 Hz, 3H). ¹³C NMR (150 MHz, CDCl₃): δ 161.83, 161.71,
45
46 148.38, 148.10, 147.09, 146.89, 136.67, 136.44, 128.72, 128.69, 127.28, 127.08,
47
48 125.67, 124.53, 122.24, 121.95, 121.89, 121.80, 119.44, 119.16, 118.83, 118.76,
49
50 115.50, 114.45, 111.77, 111.52, 111.45, 111.41, 111.17, 111.11, 64.52, 64.33, 56.11,
51
52 55.95, 50.43, 40.32, 36.96, 36.26, 34.29, 29.39, 27.57, 22.27, 22.12, 14.77, 14.68.
53
54
55
56
57
58
59
60

38

1
2
3
4 HRMS (ESI): exact mass calculated for $C_{23}H_{27}N_2O_3^+$ $[M+H]^+$ 379.2016, found
5
6
7 379.2011.

8
9
10 **(S)-1-(2-(1*H*-indol-3-yl)ethyl)-7-(cyclopropylmethoxy)-6-methoxy-3,4-**
11
12 **dihydroisoquinoline-2(1*H*)-methanal (21).** This compound (a white solid) was
13
14 prepared by replacement of **5a** with **6j** using a similar synthetic procedure of product
15
16
17
18
19 **2. 1H NMR** (400 MHz, $CDCl_3$): δ 8.28, 8.20 (2 \times s, 1H), 8.17, 8.09 (2 \times s, 1H), 7.62,
20
21 7.57 (2 \times d, $J=7.9, 7.9$ Hz, 1H), 7.38, 7.36 (2 \times d, $J=8.1, 8.1$ Hz, 1H), 7.24 – 7.16 (m,
22
23 1H), 7.15 – 7.03 (m, 1H), 7.02 (s, 1H), 6.58, 6.55 (2 \times s, 1H), 6.43, 6.42 (2 \times s, 1H),
24
25 5.48-5.40, 4.58-4.48 (2 \times m, 1H), 4.45-4.34, 3.76-3.67 (2 \times m, 1H), 3.83 (s, 3H), 3.76
26
27 – 3.66 (m, 1H), 3.66 – 3.61 (m, 1H), 3.62-3.52, 3.17-3.07 (2 \times m, 1H), 3.00 – 2.62 (m,
28
29 4H), 2.32 – 2.15 (m, 2H), 1.86-1.65(m, 1H), 0.68 – 0.51 (m, 2H), 0.29 (m, 2H). ^{13}C
30
31 **NMR** (125 MHz, $CDCl_3$): δ 161.85, 161.72, 148.67, 148.38, 147.32, 147.10, 136.68,
32
33 136.45, 128.73, 128.68, 127.28, 127.07, 125.98, 124.84, 122.24, 121.96, 121.90,
34
35 121.82, 119.42, 119.14, 118.83, 118.73, 115.46, 114.42, 112.33, 112.07, 111.98,
36
37 111.75, 111.42, 111.18, 74.33, 74.08, 56.06, 55.99, 50.42, 40.33, 36.87, 36.24, 34.30,
38
39 29.41, 27.58, 22.26, 22.07, 10.29, 10.23, 3.42, 3.40, 3.33. HRMS (ESI): exact mass
40
41 calculated for $C_{25}H_{29}N_2O_3^+$ $[M+H]^+$ 405.2100, found 405.2163.
42
43
44
45
46
47
48
49
50
51
52

53 **Virtual Screening.** Virtual screening on our in-house berberine analogues library
54
55 containing 500 compounds was carried out with the use of the structure of PDE4D
56
57 catalytic domain (PDB ID: 1TBB).³¹ The protein was prepared using Protein
58
59
60

1
2
3
4 Preparation and Grid Preparation tools in the Schrödinger Maestro interface (Maestro,
5
6 version 10.2, Schrödinger, LLC, New York, NY, 2015). The Glide docking module in
7
8 Schrödinger suite 2015-2 was applied and Standard Precision calculations with default
9
10 settings were performed (Glide, version 6.7, Schrödinger, LLC, New York, NY,
11
12 2015).³² The OPLS-2005 force field was used for docking.³³ The resulting top 30
13
14 ranked compounds were reserved for test with the enzymatic activity assay.
15
16
17
18
19
20
21

22 **Protein Purification and Crystallization.** Production of the catalytic domain of
23
24 recombinant human PDE4D and PDE5A is as follows. Briefly, cDNA fragments
25
26 encoding catalytic domain of PDE4D (86-413), PDE5A (535-860), PDE7A (130-482),
27
28 PDE9A (181-506) and PDE10A (439-766) were cloned into the vector pET15b and the
29
30 protein was expressed in *E.coli* BL21 (DE3). The expressed protein was passed through
31
32 a Ni-NTA column (GE), and further purified by Q-Sepharose and Superdex200 (GE
33
34 Healthcare). The recombinant PDE4D with a purity of > 95% was concentrated to 12
35
36 mg/mL for crystallization. Crystallization of apo PDE4D was performed at 4 °C using
37
38 the hanging drop vapor-diffusion method, by mixing equal volume (1.5 μ L:1.5 μ L) of
39
40 the protein and crystallization solution (18% (w/v) PEG 3350, 0.1 M HEPES (pH 7.0),
41
42 0.2 M MgCl₂, 10% (v/v) isopropanol, 30% (v/v) ethylene glycol). Crystals were formed
43
44 within 3 days and then soaked into crystallization buffer with 5-10 mM compounds for
45
46 6 h. Using commercial perfluoropolyether cryo oil (PFO) as croprotectant, crystals were
47
48 flash-frozen into liquid nitrogen.
49
50
51
52
53
54
55
56
57
58
59
60

1
2
3
4 **Structure Determination and Refinement.** X-ray diffraction data were collected at
5
6
7 beamline BL17U1 or BL19U1 at the Shanghai Synchrotron Radiation Facility
8
9 (SSRF).³⁴ The data were processed with HKL3000. The structure was solved by
10
11 molecular replacement using the program CCP4 with a search model of PDB code
12
13 1TBB.^{31,35} The models were built using coot and refined with a simulated-annealing
14
15 protocol implemented in the program PHENIX.^{36,37} Data collection and refinement
16
17 statistics of 10 solved structures are shown in Table S1.
18
19
20
21
22
23

24 **Isothermal Titration Calorimetry (ITC) Measurements.** All measurements were
25
26 performed by iTC200 calorimeter (General Electric Co.) in an ITC buffer (25 mM
27
28 HEPES pH 7.0, 100 mM NaCl, 0.1 mM EDTA, 1 mM MgCl₂) while stirring at 800
29
30 rpm. The stock solution of compounds and the catalytic domain of PDE4D were diluted
31
32 with the ITC buffer to a compound concentration of 0.5-2 mM and a protein
33
34 concentration of 50-500 μM before titrations. The final concentration of DMSO in the
35
36 reaction buffer is less than 2% of the total volume. Compound **4** was titrated into the
37
38 protein solution while other compounds were titrated by the protein solution. All
39
40 titrations were performed using an initial injection of 0.4 μL followed by 19 identical
41
42 injections of 2 μL with a duration of 4 seconds per injection and a spacing of 120
43
44 seconds between injections. The last five data points were averaged and subtracted from
45
46 each titration to account for the heat of dilution. Additional background experiments
47
48 where buffer was titrated into the protein solution revealed no significant shift in the
49
50
51
52
53
54
55
56
57
58
59
60

1
2
3
4 baseline during the course of the measurements. Each assay was carried out in three
5
6 independent experiments.
7
8
9

10 **PDEs Enzymatic Assay.** The activity of the purified catalytic domain of PDE4D as
11 well as PDE5A and other PDEs purchased from BPS Bioscienc were monitored by
12 measuring the hydrolysis of [³H]-cAMP or [³H]-cGMP into [³H]-AMP or [³H]-GMP
13 using a phosphodiesterase scintillation proximity assay (SPA). The protein was diluted
14 using an assay buffer (50 mM Tris pH 7.5, 8.3 mM MgCl₂, 1.7 mM EGTA) to a
15 concentration of 1-2 nM. Compounds were resuspended in DMSO (10% (v/v) in the
16 final concentration) at a stock concentration of 1 mM and then tested at different
17 concentrations varying from 500 μM to 10 nM. The reaction assay was initiated by
18 successively adding 80 μL of protein solution, 10 μL of test compound and 10 μL of
19 [³H]-cAMP or [³H]-cGMP (0.5 μCi/mL) in a “low binding” plate and all reactions were
20 carried out in duplicate. The plate was incubated at 30 °C for 30 min. Then the reaction
21 was stopped by addition of 50 μL of phosphodiesterase SPA beads (RPNQ0150,
22 PerkinElmer Inc.). All plates were settled for 20 minutes before being counted with a
23 MicroBeta² (PerkinElmer Inc.) counter. For the measurement of inhibitory activity of
24 every compound against PDE4D, at least three independent experiments were
25 performed for the determination of IC₅₀ values. At least eight concentrations of a
26 compound were used to calculate IC₅₀ values, each concentration in triplicate. All
27 experimental data were analyzed by using GraphPad Prism, version 8.0 (GraphPad Inc.).
28
29
30
31
32
33
34
35
36
37
38
39
40
41
42
43
44
45
46
47
48
49
50
51
52
53
54
55
56
57
58
59
60

1
2
3
4 **PDE4 Activity Cell Assay.** Inhibition of the TNF- α production by tested compounds
5
6 were measured in lipopolysaccharide (LPS, Sigma) stimulated human peripheral blood
7
8 mononuclear cells (PBMCs) as previously reported.³⁸ Human PBMCs extracted by
9
10 Ficoll-Paque PLUS (GE Healthcare) from human whole blood gifted by Shanghai
11
12 blood center. Cells ($8 \cdot 10^5$ cells/mL) were cultured in RPMI medium 1640 (Gibco)
13
14 supplemented with 10% FBS (Gibco), 2 mM L-glutamine (Gibco), 100 U/mL penicillin
15
16 and 100 ug/mL streptomycin (Gibco). Test compounds were added to human PBMCs
17
18 1 h prior to the addition of LPS. The final DMSO concentration was 0.2%. Human
19
20 PBMCs were stimulated with LPS for 18-20 h at 37 °C with 5% CO₂. Supernatants were
21
22 then harvested and determined by TNF- α ELISA Kit (Life technologies) and measured
23
24 on Bio-Tek Synergy4 plate reader. For the measurement of inhibitory activity of every
25
26 compound against the TNF- α production in hPBMC, at least three independent
27
28 experiments were performed for the determination of IC₅₀ values. At least eight
29
30 concentrations of a compound were used to calculate IC₅₀ values, each concentration in
31
32 triplicate. All experimental data were analyzed by using GraphPad Prism, version 8.0
33
34 (GraphPad Inc.).
35
36
37
38
39
40
41
42
43
44
45
46
47
48

49 **Caco-2 Permeability Assay.** The Caco-2 monolayer assays were performed on
50
51 compound **16** and apremilast by using the standard procedure as previously reported.³⁹
52
53 Briefly, the compounds transport from the apical side to the basolateral side (A-B) and
54
55 from the opposite direction (B-A) were measured simultaneously under the same
56
57 conditions. Propranolol and nadolol were used as the hypertonic and hypotonic control,
58
59
60

1
2
3
4 respectively. Digoxin was used as the positive control for Pgp-mediated drug efflux.
5
6
7 After washing the monolayer with HBSS (Hanks' Balanced Salt Solution, Sigma-
8
9 Aldrich) three times, the compounds were diluted and added to the appropriate well
10
11 (pH 6.8 for the apical side and pH 7.4 for the basolateral side). The plate was incubated
12
13 at 37°C for 95 min. Samples were collected from the donor side at 5 and 95 min and
14
15 from the receiver side at 35 and 95 min post incubation. The concentration of samples
16
17 was measured by LC-MS/MS. Mean values are the average of three independent
18
19 experiments and each was performed in triplicate.
20
21
22
23
24
25
26

27 **Calcium Mobilization Assay.** HEK293 cells stably expressing G α 16 with either
28
29 dopamine D1 or D2 receptor were seeded onto 96-well plates and incubated for 24 h.
30
31 Cells were loaded with 2 μ M fluo-4 AM in HBSS at 37 °C for 45 min. In the agonist
32
33 assay, the excess dye was removed and 50 μ L HBSS was added, and 25 μ L HBSS
34
35 containing compound **16**, dopamine (a positive control), or DMSO (a negative control)
36
37 was added using a FlexStation microplate reader. Meanwhile, the intracellular calcium
38
39 change was recorded at an excitation wavelength of 485 nm and an emission
40
41 wavelength of 525 nm. In the antagonist assay, the excess dye was removed and 50 μ L
42
43 HBSS containing compound **16**, SKF83566 (antagonist of D1 receptor as a positive
44
45 control), Eticloprice (antagonist of D2 receptor as a positive control) or DMSO (a
46
47 negative control) was added. After incubation at room temperature 10 min, 25 μ L HBSS
48
49 containing dopamine was dispensed into wells using a FlexStation microplate reader,
50
51 and intracellular calcium change was recorded at an excitation wavelength of 485 nm
52
53
54
55
56
57
58
59
60

1
2
3
4 and an emission wavelength of 525 nm. Data are mean values of three independent
5
6 experiments and each was performed in triplicate.
7
8
9

10
11 **hERG Inhibition Assay.** The hERG inhibition effect of compound **16** was measured
12
13 with QPatch automated patch-clamp technology in the hERG expressing CHO cell line
14
15 as previously reported.⁴⁰ In brief, the cells were grown until the density ranged within
16
17 2-5 x 10⁶ cells/mL for further experiment. The cells were voltage clamped at a holding
18
19 potential of -80 mV. The hERG current was activated by depolarizing at +20 mV for 5
20
21 s, after which the current was taken back to -50 mV for 5 s to remove the inactivation
22
23 and observe the deactivating tail current. The maximum amount of tail current was used
24
25 to determine hERG current amplitude. Compound **16** was diluted freshly in the external
26
27 solution to the desired concentrations. After achieving break-in (whole-cell)
28
29 configuration, the cells were recorded for 120 s to assess current stability. The voltage
30
31 protocol described above was then applied to the cells every 20 s throughout the whole
32
33 procedure. Only cells with stable currents were allowed to enter the drug-addition
34
35 procedure. External solution containing 0.1% DMSO (vehicle) was applied to the cells
36
37 to establish the baseline. After allowing the current to stabilize for 3 min, compound **16**
38
39 was added until the compound's effect reached a steady state or for a maximum of 3
40
41 min. Washout with external solution might be performed until the recovery of the
42
43 current reached a steady state. Positive control cisapride was used in the experiments
44
45 to ensure the normal response and quality of the cells. For IC₅₀ measurement, one
46
47 independent experiment with at least six concentrations of the compound was
48
49
50
51
52
53
54
55
56
57
58
59
60

performed, and three cells were patched for each concentration.

Pharmacokinetic Profiles in SD Rats. Six 5-6-week male Sprague-Dawley rats, weighting 150-200 g each, were purchased from Shanghai Sippr-BK laboratory animal Co. Ltd. (Shanghai, China). Following experiments were approved by the Bioethics Committee of the Shanghai Institute of Materia Medica, Chinese Academy of Sciences (IACUC: 2018-03-TW-05). Six Sprague-Dawley rats were randomly divided into two groups. Compound **16** was first dissolved in phosphate buffered saline containing 5% DMSO and 5% tween-80, and then administered orally (25 mg/kg) and intravenously (10 mg/kg) to a group of three rats after fasting for 12 h with free access to water. Blood samples were collected at nine time points (0, 0.25, 0.5, 1.0, 2.0, 4.0, 6.0, 8.0, 24h) from three rats at each time point. For measurements, blood samples (300 μ L) were collected in heparinized tubes and immediately separated by centrifugation at 11000 rpm for 5 min. Plasma was transferred into polypropylene tubes and put in the freezer at -20 °C. Plasma concentrations of **16** were analyzed using a LC-MS/MS (Agilent 1260 Infinity LC system and Agilent 6460 Triple Quad Mass Spectrometer System).

In Vivo Pharmacology

Animals. Inbred 6-8-week-old female BALB/c mice were purchased from Shanghai Lingchang Biotechnology Co., Ltd. (Certificate No.2013-0018, Shanghai, China). All mice were housed under specific pathogen-free conditions and raised in a 12 h light/dark cycle with humidity (60-80%) and temperature (22 ± 1 °C). Mice were

1
2
3
4 allowed to acclimatize in our facility for 1 week before any experiments. Following
5
6
7 experiments were carried out according to the National Institutes of Health Guides for
8
9
10 the Care and Use of Laboratory Animals and were approved by the Bioethics
11
12 Committee of the Shanghai Institute of Materia Medica, Chinese Academy of Sciences
13
14
15 (IACUC: 2018-03-TW-05).

16
17
18
19 **LPS-Induced Inflammation Model.** Female BALB/c mice were orally
20
21 administrated with apremilast (1 mg/kg), compound **16** (1 mg/kg) and vehicle (0.5%
22
23 sodium carboxymethylcellulose and 0.25% tween-80) 1.5 h before intraperitoneally
24
25 injection with a dose of 5 mg/kg of LPS. Serum and spleen homogenates were collected
26
27
28 2 h after LPS sensitization for cytokines detection.

29
30
31
32
33
34 **ELISA.** Cytokines in serum and spleen homogenates of each mouse from all groups
35
36 (n = 6 mice per group) were assayed in duplicate by using mouse IL-6, IL-10, IL-12p40
37
38 and TNF- α ELISA kits according to the manufacturer's instructions. All ELISA
39
40 quantification kits were obtained from BD Pharmingen (San Diego, CA, USA). The
41
42 capture antibodies were precoated onto 96-well high binding microplates (Corning, NY,
43
44 USA) overnight at 4 °C. After washing three times with wash buffer, add mouse serum
45
46 and spleen homogenates (50 μ L per well) and incubate 2 h at room temperature. Then,
47
48 the detection antibodies were linked to all samples and the signaling were amplified by
49
50 Streptavidin-HRP (horseradish peroxidase) incubation, in the presence of TMB (3, 3',
51
52 5, 5'-tetramethylbenzidine) substrate buffer and H₂SO₄ stop solution. The absorbance
53
54
55
56
57
58
59
60

1
2
3
4 values at 450 nm were collected by a microplate reader (Molecular Devices, Sunnyvale,
5
6 CA, USA) and the cytokine concentrations were acquired from the standard curve using
7
8 log-log regression analysis.
9
10

11
12
13 **IMQ-Induced Psoriasis-like Skin Lesions.** Female BALB/c mice were randomly
14
15 divided into 4 groups (n = 6): normal, IMQ (IMQ-applied only), IMQ + apremilast
16
17 (IMQ with 25 mg/kg apremilast), IMQ + compound **16** (IMQ with 25 mg/kg **16**). The
18
19 skin inflammation was triggered by receiving a daily topical dose of 62.5 mg of IMQ
20
21 cream on their shaved back. Apremilast or compound **16** was orally applied through a
22
23 syringe with a blunt-ended curved feeding tube. For topical treatment, 2% ointment of
24
25 compound **16** was prepared in-house and 62.5 mg of 2% ointment plus the ointment
26
27 bases were applied once daily to the mouse skin, respectively. To score the severity of
28
29 inflammation of mouse skin, an objective scoring system was developed base on the
30
31 clinical Psoriasis Area and Severity Index (PASI).⁴¹ Erythema, scaling and thickening
32
33 were scored independently from 0 to 4 as follows: 0, none; 1, slight; 2, moderate; 3,
34
35 marked; 4, very marked. The cumulative score (erythema plus scaling plus thickening)
36
37 served to indicate the severity of inflammation (scale 0-12).
38
39
40
41
42
43
44
45
46
47
48
49

50 **Statistical Analysis.** The data are presented as the mean \pm SEM. Statistical
51
52 differences were determined using one-way analysis of variance (ANOVA) with
53
54 Dunnet's multiple comparisons test with no significant variance inhomogeneity (F
55
56
57
58
59
60

1
2
3
4 achieved $p < 0.05$) using GraphPad software 6.0 (San Diego, CA, USA). P values less
5
6
7 than 0.05 were considered significant.
8
9

10 **ASSOCIATED CONTENT**

11 **Supporting Information**

12
13
14
15
16
17 Including supplementary figures of multiple X-ray crystal structures, tables, NMR
18
19
20 spectra and HRMS spectra.
21
22

23
24 Molecular formula strings and some data (CSV)

25 **Accession Codes**

26
27
28 The atomic coordinates and structure factors have been deposited into the Protein Data
29
30 Bank with accession codes 6INM (PDE4D-1), 6INK (PDE4D-2), 6IMB (PDE4D-4),
31
32
33 6IMD (PDE4D-4), 6IM6 (PDE4D-5), 6IMI (PDE4D-6), 6IMO (PDE4D-7), 6IMR
34
35
36 (PDE4D-8), 6IMT (PDE4D-15) and 6IND (PDE4D-16). Authors will release the
37
38
39 atomic coordinates and experimental data upon article publication.
40
41
42

43 **AUTHOR INFORMATION**

44 **Corresponding Authors**

45
46
47 For Y.X.: phone, +86-21-50801267; E-mail, ycxu@simm.ac.cn;

48
49 For H.L.: phone, +86-21-50807042; E-mail, hliu@simm.ac.cn;

50
51 For W.T.: phone, +86-21-50806280; E-mail, tangwei@simm.ac.cn.
52
53
54
55

56 **Author Contributions**

1
2
3
4 †These authors contributed equally. The manuscript was written through contributions
5
6
7 of all authors. All authors have given approval to the final version of the manuscript.
8

9 **Notes**

10
11
12 The authors declare no competing financial interest.
13
14

15 **ACKNOWLEDGEMENTS**

16
17
18
19
20 This study was supported by the National Key R&D Program of China (No.
21
22 2016YFA0502301), the National Science & Technology Major Project "Key New Drug
23
24 Creation and Manufacturing Program" (No. 2018ZX09711002-006-011), the Strategic
25
26 Priority Research Program of the Chinese Academy of Sciences "Personalized
27
28 Medicines—Molecular Signature-based Drug Discovery and Development" (No.
29
30 XDA12020231), the National Natural Science Foundation of China (81620108027 and
31
32 21632008), and the Science &
33
34 Technology Commission of Shanghai Municipality, China (No. 18431907100).
35
36
37
38
39
40
41
42

43 **ABBREVIATIONS USED**

44
45
46
47 PDEs, phosphodiesterases; PDE4D, phosphodiesterase 4D; cGMP, cyclic guanosine
48
49 monophosphate; cAMP, cyclic adenosine monophosphate; TCM, Traditional Chinese
50
51 medicine; C_{max}, the maximum plasma concentration; T_{max}, the time to reach C_{max};
52
53 AUC_{0-t}, total area under the plasma concentration–time curve from time zero to 24h;
54
55 AUC_{0-∞}, total area under the plasma concentration–time curve from time zero to time
56
57
58
59
60

1
2
3
4 infinity; MRT, mean retention time; $t_{1/2}$, terminal half-life; CL, plasma clearance; V_{ss} ,
5
6
7 apparent volume of distribution at steady state; F, bioavailability; IMQ, imiquimod.
8
9

10 REFERENCES

- 11
12
13
14
15 1. Maurice, D. H.; Ke, H.; Ahmad, F.; Wang, Y.; Chung, J.; Manganiello, V. C.
16
17
18 Advances in targeting cyclic nucleotide phosphodiesterases. *Nat. Rev. Drug Discov.*
19
20 **2014**, 13, 290-314.
21
22
23 2. Sun, J. G.; Deng, Y. M.; Wu, X.; Tang, H. F.; Deng, J. F.; Chen, J. Q.; Yang, S.
24
25
26 Y.; Xie, Q. M. Inhibition of phosphodiesterase activity, airway inflammation and
27
28
29 hyperresponsiveness by PDE4 inhibitor and glucocorticoid in a murine model of
30
31
32 allergic asthma. *Life Sci.* **2006**, 79, 2077-2085.
33
34 3. Zhang, K. Y.; Ibrahim, P. N.; Gillette, S.; Bollag, G. Phosphodiesterase-4 as a
35
36
37 potential drug target. *Expert Opin. Ther. Targets* **2005**, 9, 1283-1305.
38
39 4. Guo, H.; Cheng, Y.; Wang, C.; Wu, J.; Zou, Z.; Niu, B.; Yu, H.; Wang, H.; Xu, J.
40
41
42 FFPM, a PDE4 inhibitor, reverses learning and memory deficits in APP/PS1 transgenic
43
44
45 mice via cAMP/PKA/CREB signaling and anti-inflammatory effects.
46
47
48 *Neuropharmacology* **2017**, 116, 260-269.
49
50 5. Francis, S. H.; Blount, M. A.; Corbin, J. D. Mammalian cyclic nucleotide
51
52
53 phosphodiesterases: molecular mechanisms and physiological functions. *Physiol. Rev.*
54
55
56 **2011**, 91, 651-690.
57
58
59
60

- 1
2
3
4 6. Germain, N.; Corbel, M.; Belleguic, C.; Boichot, E.; Lagente, V. Effects of PDE4
5
6
7 inhibitors on lipopolysaccharide-induced priming of superoxide anion production from
8
9
10 human mononuclear cells. *Mediators Inflamm.* **2001**, 10, 117-123.
- 11
12 7. Torphy, T. J.; Barnette, M. S.; Underwood, D. C.; Griswold, D. E.; Christensen, S.
13
14 B.; Murdoch, R. D.; Nieman, R. B.; Compton, C. H. Ariflo™(SB 207499), a second
15
16
17 generation phosphodiesterase 4 inhibitor for the treatment of asthma and COPD: from
18
19
20 concept to clinic. *Pulm. Pharmacol. Ther.* **1999**, 12, 131-135.
- 21
22
23 8. Fabbri, L. M.; Beghé, B.; Yasothan, U.; Kirkpatrick, P. Roflumilast. *Nat. Rev. Drug*
24
25
26 *Discov.* **2010**, 9, 761.
- 27
28 9. Schafer, P. H.; Parton, A.; Gandhi, A. K.; Capone, L.; Adams, M.; Wu, L.; Bartlett,
29
30
31 J. B.; Loveland, M. A.; Gilhar, A.; Cheung, Y. F.; Baillie, G. S.; Houslay, M. D.; Man,
32
33
34 H. W.; Muller, G. W.; Stirling, D. I. Apremilast, a cAMP phosphodiesterase-4 inhibitor,
35
36
37 demonstrates anti-inflammatory activity in vitro and in a model of psoriasis. *Br. J.*
38
39
40 *Pharmacol.* **2010**, 159, 842-855.
- 41
42 10. Paton, D. M. Crisaborole: Phosphodiesterase inhibitor for treatment of atopic
43
44
45 dermatitis. *Drugs Today (Barc)* **2017**, 53, 239-245.
- 46
47 11. Christophers, E. Psoriasis--epidemiology and clinical spectrum. *Clin. Exp.*
48
49
50 *Dermatol.* **2001**, 26, 314-320.
- 51
52 12. Nestle, F. O.; Kaplan, D. H.; Barker, J. Psoriasis. *N. Engl. J. Med.* **2009**, 361, 496-
53
54
55 509.
- 56
57 13. Boehncke, W.-H.; Schön, M. P. Psoriasis. *The Lancet* **2015**, 386, 983-994.

- 1
2
3
4 14. Perez-Aso, M.; Montesinos, M. C.; Mediero, A.; Wilder, T.; Schafer, P. H.;
5
6
7 Cronstein, B. Apremilast, a novel phosphodiesterase 4 (PDE4) inhibitor, regulates
8
9 inflammation through multiple cAMP downstream effectors. *Arthritis. Res. Ther.* **2015**,
10
11
12 17, 249.
13
14
15 15. Cheape, A. C.; Murrell, D. F. 2% Crisaborole topical ointment for the treatment of
16
17 mild-to-moderate atopic dermatitis. *Expert Rev. Clin. Immunol.* **2017**, 13, 415-423.
18
19
20 16. Rodrigues, T.; Reker, D.; Schneider, P.; Schneider, G. Counting on natural
21
22 products for drug design. *Nat. Chem.* **2016**, 8, 531-541.
23
24
25 17. Karaosmanoglu, K.; Sayar, N. A.; Kurnaz, I. A.; Akbulut, B. S. Assessment of
26
27 berberine as a multi-target antimicrobial: a multi-omics study for drug discovery and
28
29 repositioning. *OMICS* **2014**, 18, 42-53.
30
31
32
33 18. Bandyopadhyay, S.; Patra, P. H.; Mahanti, A.; Mondal, D. K.; Dandapat, P.;
34
35 Bandyopadhyay, S.; Samanta, I.; Lodh, C.; Bera, A. K.; Bhattacharyya, D.; Sarkar, M.;
36
37 Baruah, K. K. Potential antibacterial activity of berberine against multi drug resistant
38
39 enterovirulent *Escherichia coli* isolated from yaks (*Capra hircus*) with
40
41 haemorrhagic diarrhoea. *Asian Pac. J. Trop. Med.* **2013**, 6, 315-319.
42
43
44
45 19. Xu, L.; Zheng, X.; Wang, Y.; Fan, Q.; Zhang, M.; Li, R.; Ye, J.; Wu, X.; Zhao, W.;
46
47
48 Zhang, Y. Berberine protects acute liver failure in mice through inhibiting inflammation
49
50 and mitochondria-dependent apoptosis. *Eur. J. Pharmacol.* **2018**, 819, 161-168.
51
52
53
54
55
56
57
58
59
60

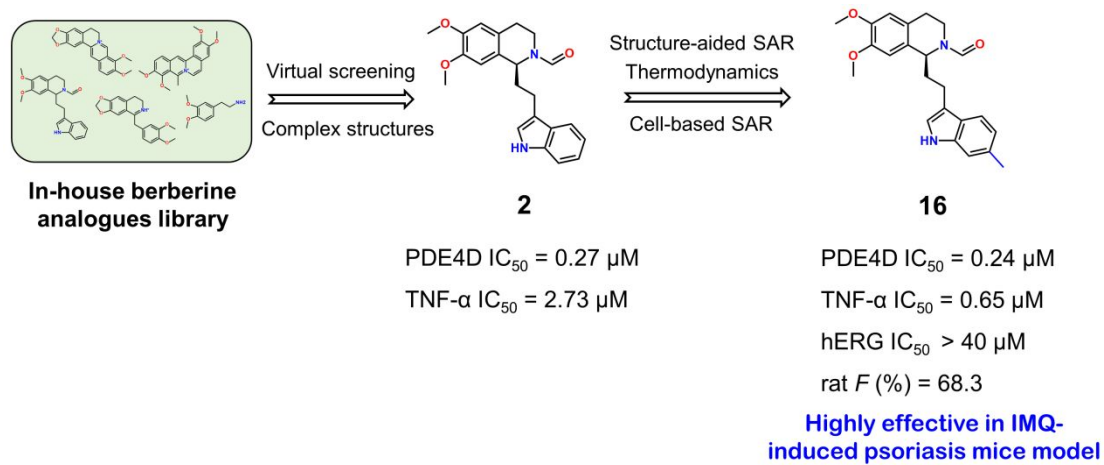
- 1
2
3
4 20. Zhang, H.; Shan, Y.; Wu, Y.; Xu, C.; Yu, X.; Zhao, J.; Yan, J.; Shang, W. Berberine
5
6 suppresses LPS-induced inflammation through modulating Sirt1/NF-kappaB signaling
7
8 pathway in RAW264.7 cells. *Int. Immunopharmacol.* **2017**, 52, 93-100.
9
10
11
12 21. Zou, K.; Li, Z.; Zhang, Y.; Zhang, H. Y.; Li, B.; Zhu, W. L.; Shi, J. Y.; Jia, Q.; Li,
13
14 Y. M. Advances in the study of berberine and its derivatives: a focus on anti-
15
16 inflammatory and anti-tumor effects in the digestive system. *Acta Pharmacol. Sin.* **2017**,
17
18 38, 157-167.
19
20
21
22 22. Hur, J. M.; Hyun, M. S.; Lim, S. Y.; Lee, W. Y.; Kim, D. The combination of
23
24 berberine and irradiation enhances anti-cancer effects via activation of p38 MAPK
25
26 pathway and ROS generation in human hepatoma cells. *J. Cell. Biochem.* **2009**, 107,
27
28 955-964.
29
30
31
32
33 23. Mang, S.; Bucher, H.; Nickolaus, P. Development of a scintillation proximity assay
34
35 (SPA) based, high throughput screening feasible method for the identification of
36
37 PDE12 activity modulators. *Curr. Drug Discov. Technol.* **2016**, 13, 144-151.
38
39
40
41 24. O'Neill, L. A. Targeting signal transduction as a strategy to treat inflammatory
42
43 diseases. *Nat. Rev. Drug Discov.* **2006**, 5, 549-563.
44
45
46
47 25. Akama, T.; Baker, S. J.; Zhang, Y.-K.; Hernandez, V.; Zhou, H.; Sanders, V.;
48
49 Freund, Y.; Kimura, R.; Maples, K. R.; Plattner, J. J. Discovery and structure–activity
50
51 study of a novel benzoxaborole anti-inflammatory agent (AN2728) for the potential
52
53 topical treatment of psoriasis and atopic dermatitis. *Bioorg. Med. Chem. Lett.* **2009**, 19,
54
55 2129-2132.
56
57
58
59
60

- 1
2
3
4 26. Kawano, M.; Takagi, R.; Kaneko, A.; Matsushita, S. Berberine is a dopamine D1-
5 and D2-like receptor antagonist and ameliorates experimentally induced colitis by
6
7 and D2-like receptor antagonist and ameliorates experimentally induced colitis by
8
9 suppressing innate and adaptive immune responses. *J. Neuroimmunol.* **2015**, 289, 43-
10
11 55.
12
13
14
15 27. Jones, K. A.; Garbati, N.; Zhang, H.; Large, C. H. Automated patch clamping using
16
17 the QPatch. *Methods. Mol. Biol.* **2009**, 565, 209-223.
18
19
20
21 28. Blanque, R.; Meakin, C.; Millet, S.; Gardner, C. R. Selective enhancement of LPS-
22
23 induced serum TNF-alpha production by carrageenan pretreatment in mice. *Gen.*
24
25 *Pharmacol.* **1998**, 31, 301-306.
26
27
28
29 29. Flutter, B.; Nestle, F. O. TLRs to cytokines: mechanistic insights from the
30
31 imiquimod mouse model of psoriasis. *Eur. J. Immunol.* **2013**, 43, 3138-3146.
32
33
34 30. Gilliet, M.; Conrad, C.; Geiges, M.; Cozzio, A.; Thurlimann, W.; Burg, G.; Nestle,
35
36 F. O.; Dummer, R. Psoriasis triggered by toll-like receptor 7 agonist imiquimod in the
37
38 presence of dermal plasmacytoid dendritic cell precursors. *Arch. Dermatol.* **2004**, 140,
39
40 1490-1495.
41
42
43
44 31. Zhang, K. Y.; Card, G. L.; Suzuki, Y.; Artis, D. R.; Fong, D.; Gillette, S.; Hsieh,
45
46 D.; Neiman, J.; West, B. L.; Zhang, C.; Milburn, M. V.; Kim, S. H.; Schlessinger, J.;
47
48 Bollag, G. A glutamine switch mechanism for nucleotide selectivity by
49
50 phosphodiesterases. *Mol. Cell.* **2004**, 15, 279-286.
51
52
53
54 32. Friesner, R. A.; Banks, J. L.; Murphy, R. B.; Halgren, T. A.; Klicic, J. J.; Mainz,
55
56 D. T.; Repasky, M. P.; Knoll, E. H.; Shelley, M.; Perry, J. K.; Shaw, D. E.; Francis, P.;

- 1
2
3
4 Shenkin, P. S. Glide: a new approach for rapid, accurate docking and scoring. 1.
5
6 method and assessment of docking accuracy. *J. Med. Chem.* **2004**, 47, 1739-1749.
7
8
9 33. Jorgensen, W. L.; Tirado-Rives, J. The OPLS [optimized potentials for liquid
10 simulations] potential functions for proteins, energy minimizations for crystals of cyclic
11 peptides and crambin. *J. Am. Chem. Soc.* **1988**, 110, 1657-1666.
12
13
14 34. Wang, Q.-S.; Zhang, K.-H.; Cui, Y.; Wang, Z.-J.; Pan, Q.-Y.; Liu, K.; Sun, B.;
15 Zhou, H.; Li, M.-J.; Xu, Q.; Xu, C.-Y.; Yu, F.; He, J.-H. Upgrade of macromolecular
16 crystallography beamline BL17U1 at SSRF. *Nucl. Sci. Tech.* **2018**, 29, 68.
17
18
19 35. Collaborative Computational Project, N. The CCP4 suite: programs for protein
20 crystallography. *Acta Crystallogr. D. Biol. Crystallogr.* **1994**, 50, 760-763.
21
22
23 36. Emsley, P.; Cowtan, K. Coot: model-building tools for molecular graphics. *Acta*
24 *Crystallogr. D. Biol. Crystallogr.* **2004**, 60, 2126-2132.
25
26
27 37. Adams, P. D.; Grosse-Kunstleve, R. W.; Hung, L.-W.; Ioerger, T. R.; McCoy, A.
28 J.; Moriarty, N. W.; Read, R. J.; Sacchettini, J. C.; Sauter, N. K.; Terwilliger, T. C.
29 PHENIX: building new software for automated crystallographic structure
30 determination. *Crystallogr. D. Biol. Crystallogr.* **2002**, 58, 1948-1954.
31
32
33 38. Periasamy, R.; Kalal, I. G.; Krishnaswamy, R.; Viswanadha, V. Quercetin protects
34 human peripheral blood mononuclear cells from OTA-induced oxidative stress,
35 genotoxicity, and inflammation. *Environ. Toxicol.* **2016**, 31, 855-865.
36
37
38
39
40
41
42
43
44
45
46
47
48
49
50
51
52
53
54
55
56
57
58
59
60

- 1
2
3
4 39. Skolnik, S.; Lin, X.; Wang, J.; Chen, X.-H.; He, T.; Zhang, B. Towards prediction
5
6 of in vivo intestinal absorption using a 96-Well Caco-2 assay. *J. Pharm. Sci.* **2010**, *99*,
7
8 3246-3265.
9
10
11
12 40. Zhou, S.; Duan, Y.; Wang, J.; Zhang, J.; Sun, H.; Jiang, H.; Gu, Z.; Tong, J.; Li, J.;
13
14 Li, J.; Liu, H. Design, synthesis and biological evaluation of 4,7,12,12a-tetrahydro-5H-
15
16 thieno[3',2':3,4]pyrido[1,2-b]isoquinolines as novel adenosine 5' -
17
18 monophosphate-activated protein kinase (AMPK) indirect activators for the treatment
19
20 of type 2 diabetes. *Eur. J. Med. Chem.* **2017**, *140*, 448-464.
21
22
23
24
25 41. Langley, R. G.; Ellis, C. N. Evaluating psoriasis with psoriasis area and severity
26
27 index, psoriasis global assessment, and lattice system physician's global assessment. *J.*
28
29 *Am. Acad. Dermatol.* **2004**, *51*, 563-569.
30
31
32
33
34
35
36
37
38
39
40
41
42
43
44
45
46
47
48
49
50
51
52
53
54
55
56
57
58
59
60

Table of Contents Graphic



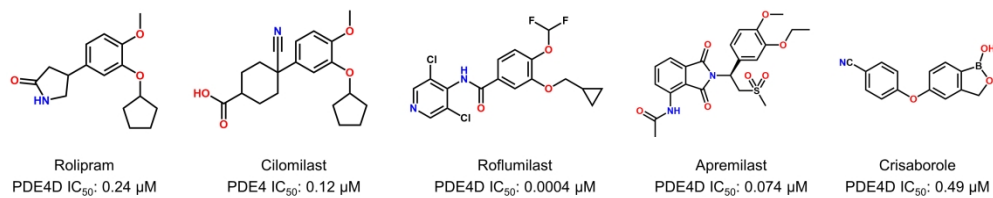


Figure 1. Structures and inhibitory activities of representative PDE4 inhibitors including three approved drugs (roflumilast, apremilast and crisaborole).

324x63mm (300 x 300 DPI)

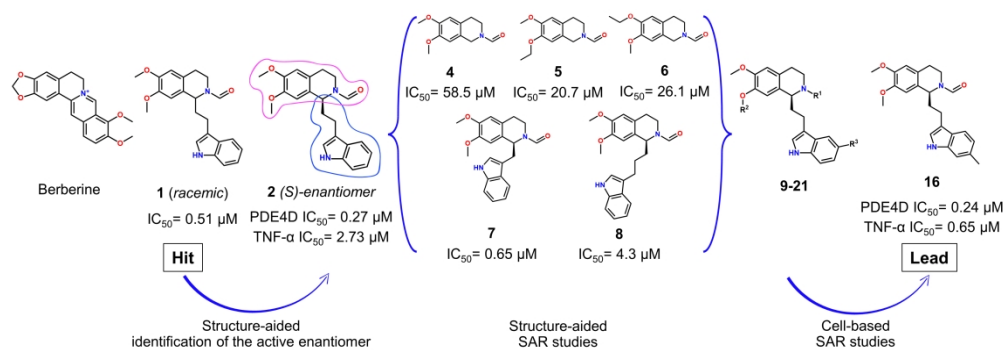


Figure 2. Structure-aided and cell-based discovery and design of the lead compound (16) based on an in-house BBR analogues library.

338x115mm (300 x 300 DPI)

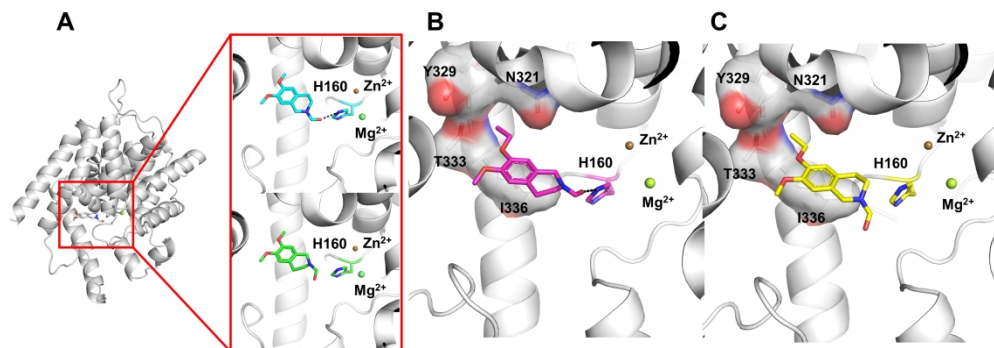


Figure 3. Crystal structures of the catalytic domain of PDE4D in complex with compounds 4 (cyan and green), 5 (magenta) and 6 (yellow). (A) Two opposite orientations of 4 were found in the binding pocket of PDE4D. (B,C) The ethoxyl groups of 5 and 6 both insert into a hydrophobic sub-pocket (the Q-pocket) formed by the sidechains of N321, Y329, T333, and I336 (grey surface). Dash lines indicate H-bonds between compounds and residues.

338x118mm (300 x 300 DPI)

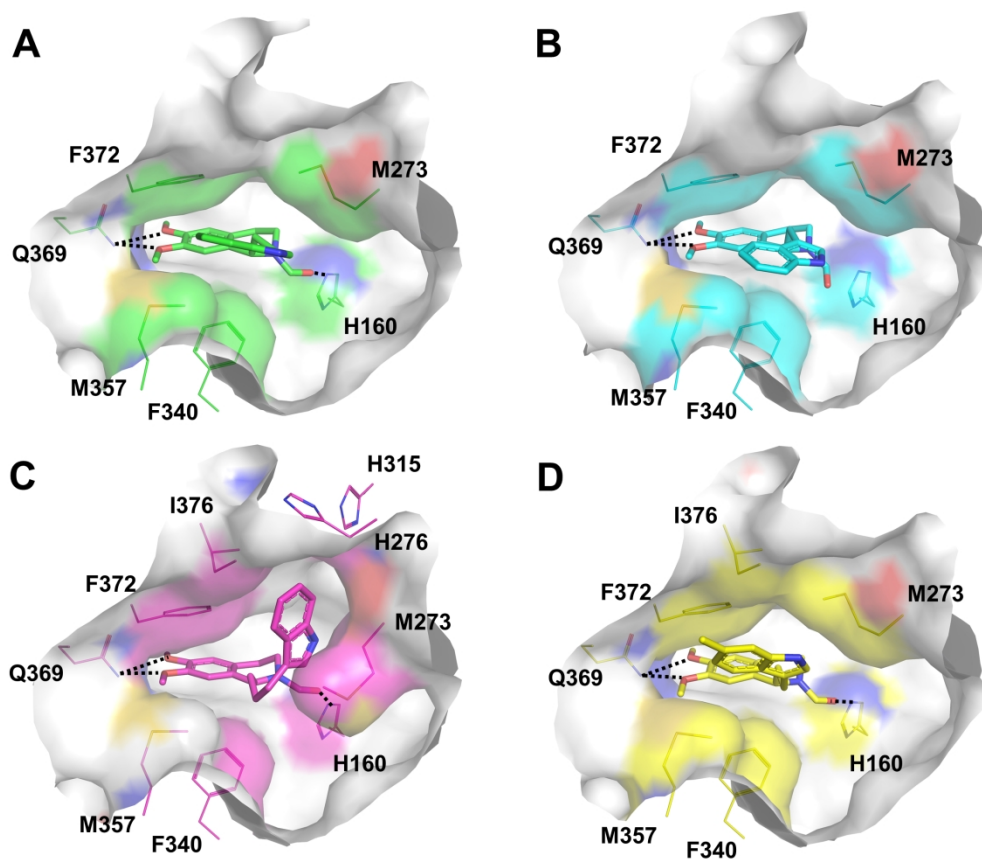


Figure 4. The effect of different linkers on orientations of the indole ring. Surface representation of the PDE4-2 (cyan, A), PDE4-7 (magenta, B), PDE4-8 (green, C), and PDE4-16 (yellow, D) complexes. Dash lines indicate H-bonds between compounds and residues.

215x190mm (300 x 300 DPI)

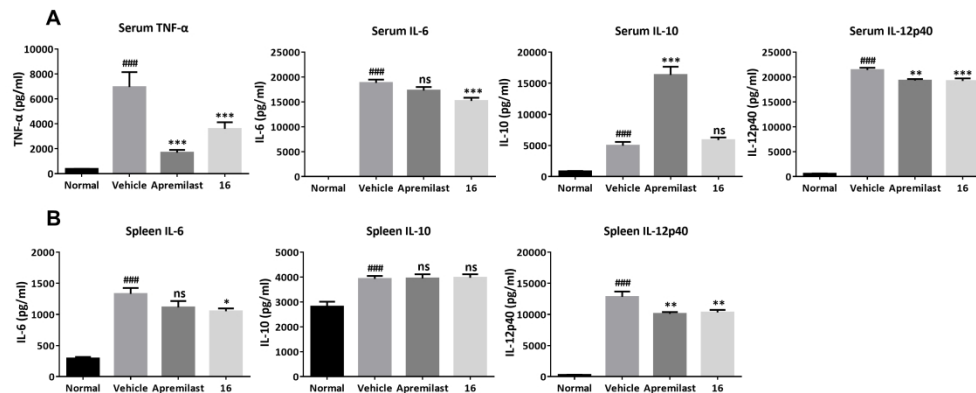


Figure 5. (A) Histograms representation of inflammation cytokines concentrations in serum of LPS-induced mice model after an oral administration of compound 16 (1 mg/kg) or apremilast (1 mg/kg) only once at 1.5 h before LPS application (n=6). (B) Similar inflammation cytokines concentration profiles in spleen at the same dose are displayed (n=6). Data are given as mean \pm S.E.M. Statistical analysis is performed by one-way ANOVA. *P < 0.05, **P < 0.01 and ***P < 0.001 compared with vehicle. #P < 0.05, ##P < 0.01 and ###P < 0.001 compared with normal.

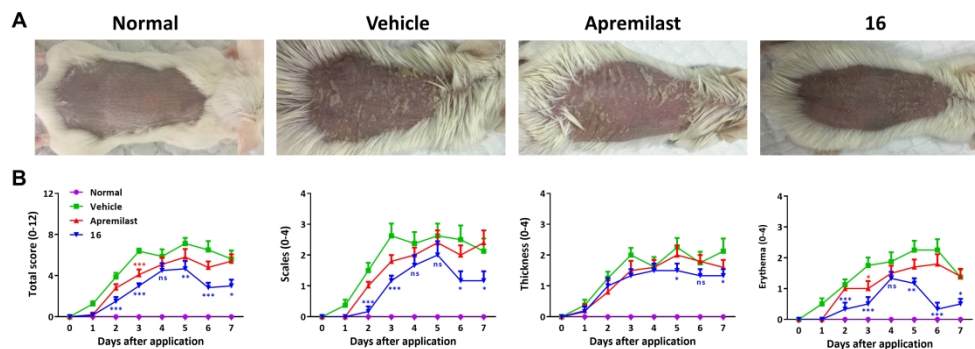


Figure 6. Efficacy of oral administration of 16 or apremilast at a dose of 25 mg/kg once daily to the IMQ-induced psoriasis-like mice. (A) A representative phenotypic manifestation of back skin in each group (n=6) after IMQ treatment for 7 days. (B) The cumulative scores were monitored daily ranging from 0 to 12, including scales, thickness and erythema. Data are given as mean \pm SEM. *P < 0.05, **P < 0.01 and ***P < 0.001, compared with vehicle.

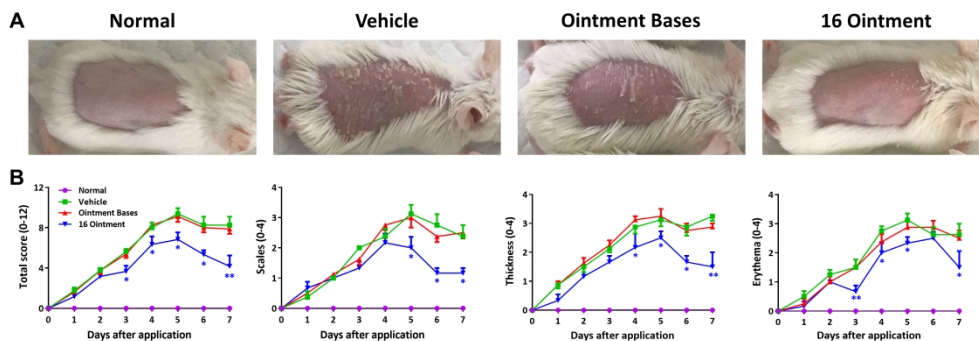


Figure 7. The therapeutic efficacy of a topical application of compound 16 in the IMQ-induced psoriasis-like mice. The cream with or without 2% of compound 16 at a dose of 62.5 mg once daily were topically applied to the back skin of the mice. (A) A representative phenotypic manifestation of back skin in each group (n=6) during 7 days of treatment with or without 16. (B) The cumulative scores were monitored daily ranging from 0 to 12, including scales, thickness and erythema. Data are given as mean \pm SEM. *P < 0.05, **P < 0.01 and ***P < 0.001, compared with vehicle.

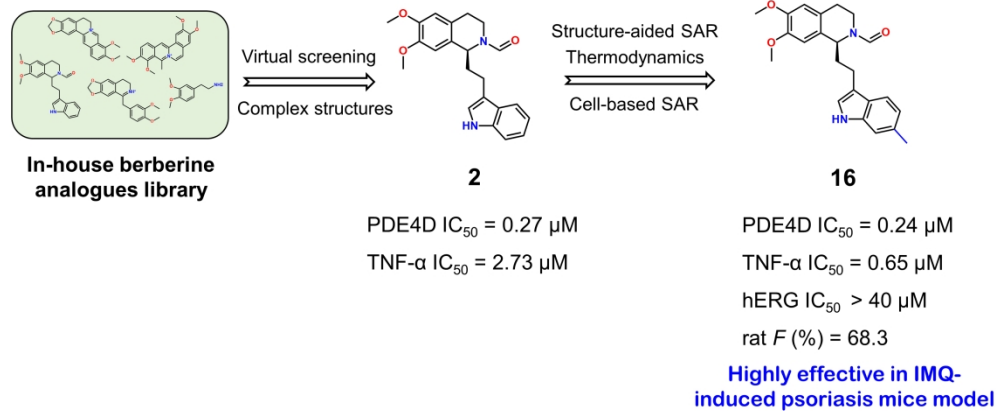


Table of Contents Graphic

270x113mm (300 x 300 DPI)